Journal of Asian Earth Sciences 147 (2017) 254–270

Contents lists available at ScienceDirect

Journal of Asian Earth Sciences

journal homepage: www.elsevier.com/locate/jseaes

Full length article

# Provenance of sediments in the Marwar Supergroup, Rajasthan, India: Implications for basin evolution and Neoproterozoic global events

Bivin G. George[a,b,*], Jyotiranjan S. Ray[a]

[a] Geosciences Division, Physical Research Laboratory, Ahmedabad 380009, India
[b] Department of Geology, The Maharaja Sayajirao University of Baroda, Vadodara 390002, India

ARTICLE INFO

*Keywords:*
Marwar Supergroup
Chhoti Khatu Tuff
Neoproterozoic
Quantitative provenance analysis
Neodymium isotopes
Western India

ABSTRACT

The Marwar Supergroup of NW India is one of the largest Neoproterozoic sedimentary successions of India. Deposited in an intracratonic sag basin, the Supergroup contains largely unmetamorphosed and undeformed fluvial and marginal marine siliciclastics, marine carbonates, and minor volcaniclastics which hold clues to the geotectonic evolution of India subsequent to the disintegration of the Rodinia and during the formation of the Gondwanaland. Here, we present age constraints for the initiation of sedimentation and evolution of the basin. The Rb-Sr whole rock isochron of a felsic tuff from the lower part of the Supergroup, yields an age of 703 ± 40 Ma, which suggests that the sedimentation in the Marwar basin started in the Cryogenian period. The result of Sr isotope stratigraphy suggests a depositional age of ~570 Ma (Late Ediacaran) for the carbonate sequences in the middle part of the Supergroup, indicating a depositional hiatus of ~100 Ma between the lower and middle Marwars. We speculate that this relapse in the sedimentation could be related to the widespread Pan-African event (Malagasy Orogeny). Provenance analysis using Neodymium (Nd) isotopes and trace elements shows that sediments in the lower Marwars were contributed by the Delhi Supergroup (~1.6 Ga), Banded Gneissic Complex-2 (> 1.8 Ga) and possibly the Erinpura Granites (~850 Ma), whereas the siliciclastics deposited in the middle and upper Marwars were predominantly sourced from the Delhi Supergroup. Interestingly, the contribution from the Malani Igneous Suite (MIS) to the sedimentation is limited only to the basal formation near the basin margin.

## 1. Introduction

The Neoproterozoic Era (1000–541 Ma) had witnessed dynamic changes in climate (Hoffman et al., 1998; Och and Shields-Zhou, 2012), life (Canfield et al., 2007; McFadden et al., 2008), and tectonics in terms of continental configurations (Collins and Pisarevsky, 2005; Meert, 2003). The supercontinent Rodinia broke apart and the stage was set for the amalgamation of Gondwanaland (Li et al., 2008). Deposition of the Marwar Supergroup of Rajasthan, western India took place during this Era. Sedimentation in the basin possibly started subsequent to the break-up of Rodinia (Roy and Jakhar, 2002) and believed to have continued through the period that saw the formation of Gondwanaland (McKenzie et al., 2011), thus making it contemporaneous with the Huqf Supergroup of Oman, Salt Range of Pakistan, Krol-Tal Groups of the Himalaya and Molo Group of Madagascar (Cozzi et al., 2012; Davis et al., 2014; Turner et al., 2014). Paleomagnetic studies within the Marwar Supergroup suggests an equatorial paleogeographic position for the Indian shield during basin development alongside the Arabian-Nubian shield, Eastern Antarctica and Australia in the Ediacaran-early Cambrian Period (Davis et al., 2014). However, an intermediate northerly latitude is also proposed for the basement of the basin; the ~750 Ma old Malani Igneous Suite (MIS), which suggests that the Indian shield along with Laurentia, Baltica, South China and Seychelles formed the western margin of the Rodinia (Gregory et al., 2009; Meert et al., 2013; Torsvik et al., 2001). Furthermore, there have been growing support for the view, from various microbially induced sedimentary structures (MISS) (Kumar and Ahmad, 2014; Sarkar et al., 2008) and Edicaran type fossils (Kumar et al., 2009) within the lower part of the Marwar Supergroup, that the sedimentation in the basin started well before the Ediacaran Period. Deposited in a shallow intracratonic sag basin, the Marwar Supergroup consists of largely unmetamorphosed and undeformed fluvial and marginal marine siliciclastics, marine carbonates and minor volcaniclastics (Paliwal, 1998; Pareek, 1981; Roy and Jakhar, 2002).

Because of its temporal occurrence and likely spatial configuration, the basin and its sedimentary record hold keys to our understanding of the post-Rodinian tectono-climatic evolution of the Indian shield. In this study, we attempt to unravel the sedimentary history of the basin

* Corresponding author at: Geosciences Division, Physical Research Laboratory, Ahmedabad 380009, India.
*E-mail address:* bivin@prl.res.in (B.G. George).

http://dx.doi.org/10.1016/j.jseaes.2017.07.027
Received 30 January 2017; Received in revised form 10 July 2017; Accepted 16 July 2017
Available online 18 July 2017

by constraining the provenance of the siliciclastic formations and siliciclastics within the carbonate formations of the Supergroup using variations in trace element contents and radiogenic isotopic (Sr-Nd) compositions as proxies. To establish the chronology of the events, we provide age constraints on deposition of various formations using Rb-Sr isochron dating of a tuff layer and $^{87}Sr/^{86}Sr$ stratigraphy of the carbonate sequences.

## 2. Geologic setting

### 2.1. Regional geology

The Aravalli Craton is generally considered to be represented by the 3.3–2.5 Ga Banded Gneissic Complex (BGC-1) in southern Rajasthan which forms the basement of subsequent magmatic activities and sedimentary deposits (Fig. 1) (Gopalan et al., 1990; Roy and Kröner, 1996; Wiedenbeck and Goswami, 1994). It consists dominantly of amphibolite to granulite grade tonalitic and granodioritic gneisses, with associated lenticular masses of amphibolite. The ancestry of BGC of central Rajasthan (BGC-2), however, remains equivocal (Fig. 1) (Bhowmik and Dasgupta, 2012; Buick et al., 2006; Tobisch et al., 1994). This slightly younger basement is exposed to the north of BGC-1. It is subdivided into (1) the Sandmata Complex consisting of granulites and (2) the Mangalwar Complex; a spatially more extensive assemblage of gneisses, meta-granitoids and minor amphibolites. The stabilization of the Aravalli Craton at ~2.5 Ga (Wiedenbeck et al., 1996) was followed by sedimentation of the Aravalli Supergroup (2.3–1.6 Ga ?) and the Delhi Supergroup (1.8–0.8 Ga ?) (Ahmad et al., 2008; Biju-Sekhar et al., 2003; Kaur et al., 2011b; McKenzie et al., 2013; Van Lente et al., 2009). A major thermal event is believed to have occurred in the Aravalli Craton at ~1.7 Ga and is manifested in most of the geochronological data reported from the region (Buick et al., 2006; Roy et al., 2005; Tobisch et al., 1994). The Delhi Supergroup is intruded by numerous granitic plutons that largely fall into two categories; (1) the older 1.7–1.8 Ga group, which is exposed mostly in the northeastern part of the Delhi Fold Belt (DFB; Biju-Sekhar et al., 2003; Choudhary, 1984; Kaur et al., 2011a, 2009, 2007) and (2) the younger (0.8–1.0 Ga) and abundant group of rocks known as the Erinpura Granites that are exposed in the southwestern part. (Choudhary, 1984; Pandit et al., 2003; Van Lente et al., 2009) A metasedimentary sequence, known as the Sirohi Group, comprising of shales and carbonates metamorphosed to lower greenschist facies, is exposed within the younger DFB granitoids (Purohit et al., 2012). The Precambrian magmatic activity in the Aravalli Craton ended with the voluminous 770–750 Ma Malani magmatism, which produced a suite of rocks that are dominated by rhyolites with minor basic volcanics and granitoids (Crawford and Compston, 1970; Gregory et al., 2009; Meert et al., 2013; Rathore et al., 1999, 1996).

### 2.2. Marwar Supergroup

The Marwar Supergroup unconformably overlies the MIS, covering an area of over 100,000 km$^2$ (Kumar, 1999) (Fig. 1). The Aravalli Mountain range, the Delhi-Lahore subsurface ridge and the Devikot-Nachna subsurface high form the boundaries of the basin in east, north and southwest, respectively (Pareek, 1984, 1981). Most of the north and northeastern parts of the basin are covered by Quaternary sand deposits. The MIS forms the basement of the Marwar basin in central

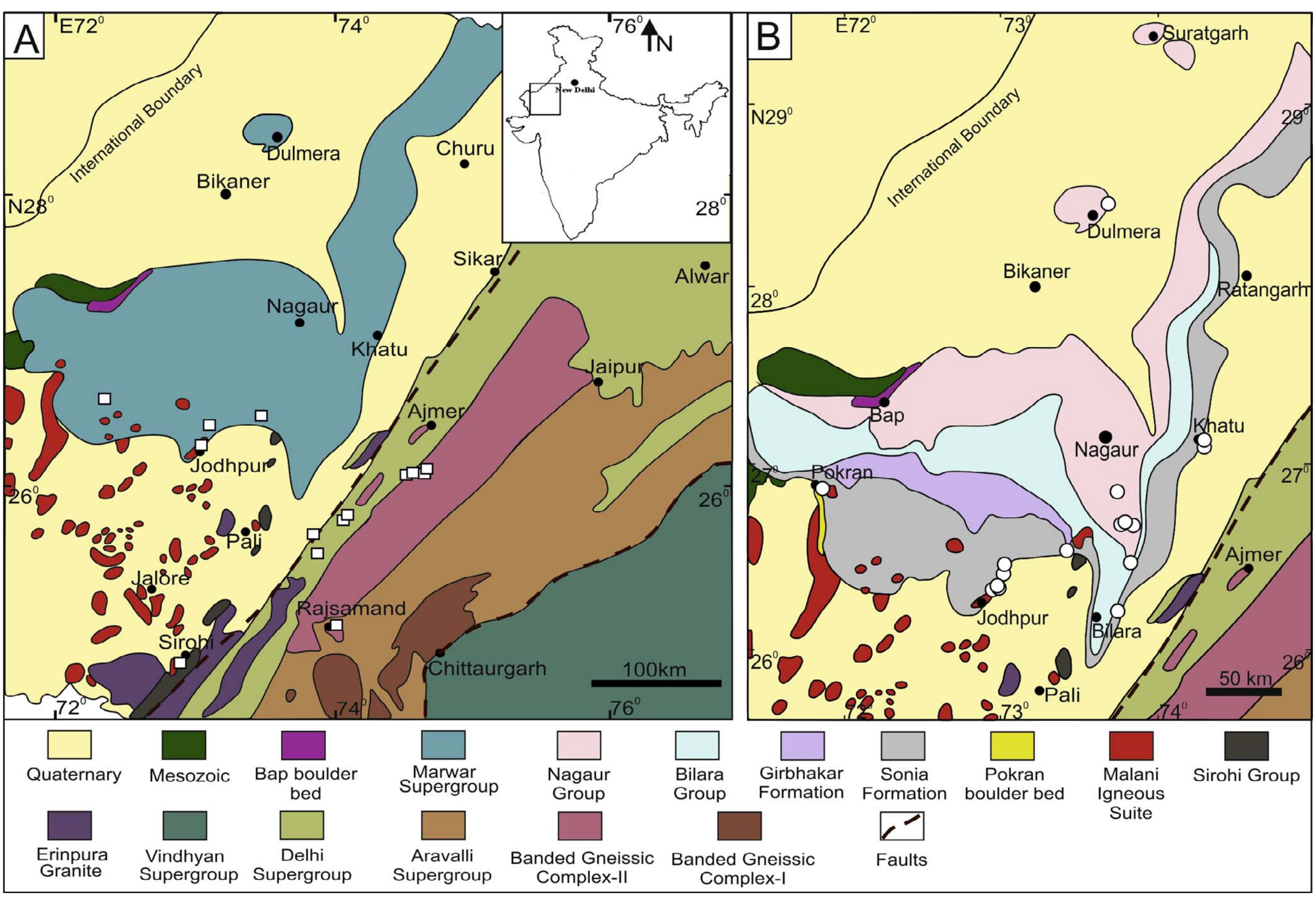


**Fig. 1.** (A) Geological map of western India showing the Marwar Supergroup and surrounding litho-tectonic units (modified after Roy and Jakhar, 2002). The study area is marked in the inset and sampling locations of the basement rocks are shown as white squares. (B) Geological map of the Marwar Supergroup with stratigraphic subdivisions (modified after Pareek, 1984). Locations of the samples from Marwar Supergroup are shown as white circles.

and western regions. The eastern Marwars are exposed near the Khatu village and are deposited over a sequence of highly deformed metsediments which belong to the ~850 Ma old Sirohi Group (Paliwal, 1998). Erinpura Granites also form the basement of the basin in certain parts of the eastern fringes (Linnemann and Sharma, 2014). The Marwar Supergroup may have a maximum thickness of 2000 m (Pareek, 1981) and is classified into three groups from bottom to top as: the Jodhpur Group, the Bilara Group and the Nagaur Group (Fig. 2). At the western margin of the basin, the unconformity between the MIS and the Marwar Supergroup is represented by the Pokaran Boulder Bed (Fig. 2). The origin and chronology of this boulder bed remains uncertain with some believing it to be of glacial origin (Chauhan et al., 2001) and others argue for a fluvial origin (Cozzi et al., 2012). The overlying Sonia Formation consists of red and white sandstones and maroon shales believed to have formed in deltaic and beach environment (Chauhan et al., 2004). The top part of the Jodhpur Group, the Girbhakar Formation is a gritty and pebbly sandstone of fluvial origin (Chauhan et al., 2004). Paliwal (1998) reported occurrences of felsic volcanics; rhyolites and alternate layers of calcareous tuff and pure ash beds sandwiched between the Sonia and Girbhakar Formations, within the Jodhpur Group in the eastern part of the basin at Chhoti Khatu village (Figs. 2 and 3). The calcareous tuff consists of angular fragments of quartz, K-feldspar, randomly oriented blades of biotite and muscovite, minor chert and glass shards in a siliceous-micritic groundmass (Fig. 3C). Volcanic debris trapped in microbialite lamellae and angular fragments of pure rhyolite are also present in the tuff. The shallow marine carbonate rocks of the Bilara Group form the middle portion of the Marwar Supergroup. It is divided, from bottom to top, into three formations: (1) The Dhanapa Formation which consists of stromatolitic dolostone, (2) the Gotan Formation that contains wavy, laminated limestone, and (3) the Pondlo Formation made entirely up of dolostone. The Bilara Group also includes subsurface evaporites (Das Gupta, 1996) which are considered to be a facies variation of the carbonates (Mazumdar and Bhattacharya, 2004; Mazumdar and Strauss, 2006). The Nagaur Group, which includes the Nagaur and Tunklian Formations, consists of braided fine to coarse grained reddish brown

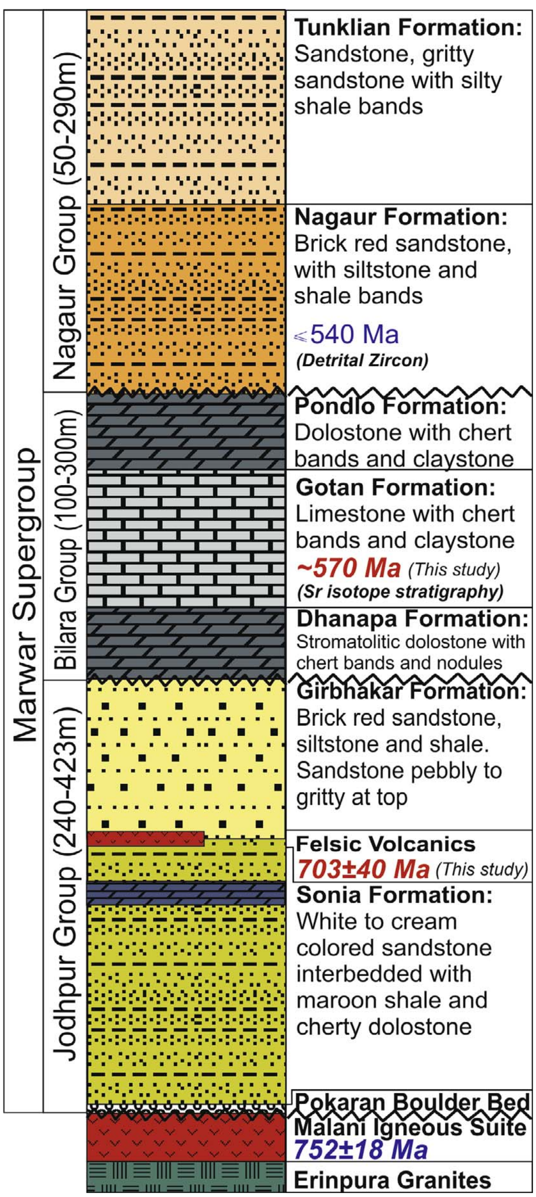


**Fig. 2.** Simplified stratigraphy of the Marwar Supergroup based on information given in Pareek (1984). Age constraints are from McKenzie et al. (2011), Meert et al. (2013) and the present study.

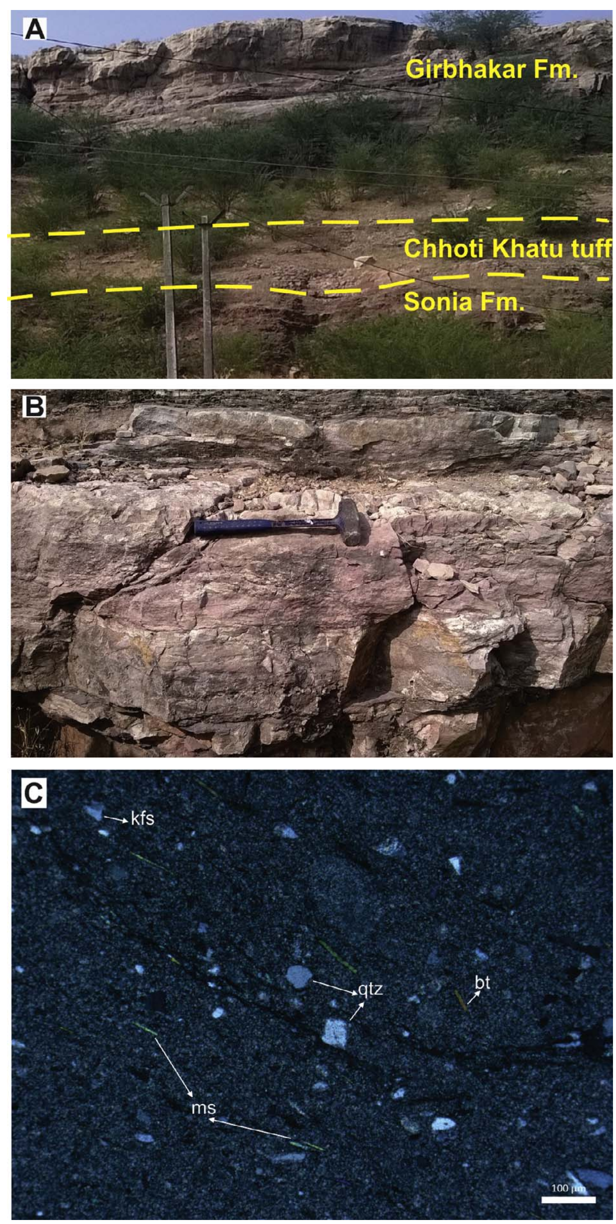


**Fig. 3.** (A) Outcrop photo of the calcareous tuff at Chhoti Khatu village, eastern Marwars. (B) A close up outcrop photo of the tuff layer. (C) Photomicrograph of the calcareous tuff under cross polarized transmitted light showing angular fragments of quartz and feldspar, blades of mica in a siliceous-micritic groundmass.

sandstones and siltstones of fluvial origin. They are unconformably overlain by the Permo-Carboniferous Bap Boulder Bed (Pandey and Bahadur, 2009).

### 2.3. Chronology of sedimentation

The Marwar Supergroup has been traditionally considered to be Neoproterozoic in age (Pandit et al., 2001). However, there were no radiometric dates available to constrain ages of deposition of various formations. The terminal dyke phase of the basement MIS has been dated to 752 ± 18 Ma (Fig. 2; Meert et al., 2013). This forms the lower time bound of the Marwar Supergroup. The current understanding of the antiquity of deposition of various groups in the basin is primarily based on biostratigraphy. Body fossils like *Hiemalora*, *Aspidella*, *Beltanelliformis minuta* (Kumar and Pandey, 2009; Raghav et al., 2005) and various microbially induced sedimentary structures (MISS) (Kumar and Ahmad, 2014; Kumar and Pandey, 2009; Sarkar et al., 2008) have been reported from the Jodhpur Group suggesting a Late Neoproterozoic sedimentation for the lower Marwars. Kumar and Pandey (2010) reported Cambrian trace fossils like *Rusophychus* and *Cruziana* from the lower part of the Nagaur Formation indicating that the Marwar sedimentation extended well into the Cambrian. Using Sr isotope stratigraphy of carbonates, Mazumdar and Strauss (2006) suggested that the Bilara Group ($^{87}Sr/^{86}Sr$ = 0.7082) was deposited during the Ediacaran to early Cambrian time. The detrital zircon age data from the sandstones of the Jodhpur Group show the youngest peak at ~750 Ma, which is essentially the age of the basement MIS and the older age peaks of ~850 Ma and ~1.8 Ga are likely from the Erinpura and BGC-2 respectively (Malone et al., 2008; Turner et al., 2014). McKenzie et al. (2011) carried out detrital zircon analysis of the Naguar Formation and reported youngest zircon ages of ~540 Ma, which can be considered as the maximum age of the Nagaur Formation (Fig. 2).

## 3. Samples and methods

We carried out extensive field work and sampling of siliciclastic sedimentary rocks, carbonates and volcaniclastics from various parts of the Marwar basin. Samples were also collected from the potential source regions of sediments; these include BGC-2, Delhi and Aravalli Supergroups, Erinpura Granites and MIS (Table 1). All siliciclastic rock samples were powdered and decarbonated using 2 N HCl before geochemical analyses. All analytical measurements were carried out at the Physical Research Laboratory, Ahmedabad. About 50 mg of each sample was dissolved using conventional HF-$HNO_3$ acid dissolution

**Table 1**
Details of the samples from the Marwar Supergroup and adjacent basement rocks.

| Sl no. | Marwar Supergroup | Sample ID | Location | Description |
|---|---|---|---|---|
| 1 | Chhoti Khatu felsic volcanics | MWR 15-3,4,5,7,8 | N 27.163°; E 74.353° | Calcareous rhyolitic tuff |
| 2 | Gotan Formation | MWR 14-17,37 | N 26.667°; E 73.733° | Siliceous limestone |
| 3 | Gotan Formation | MWR 14-79,85,95 | N 26.494°; E 73.800° | Siliceous limestone |
| 4 | Gotan Formation | MWR 14-121 | N 26.881°; E 73.518° | Siliceous limestone |
| 5 | Sonia Formation | MWR 14-1 | N 26.587°; E 73.414° | Fine-grained sandstone |
| 6 | Sonia Formation | MWR 14-126 | N 26.382°; E 73.060° | Shale |
| 7 | Sonia Formation | MWR 14-127 | N 26.382°; E 73.060° | Fine-grained sandstone |
| 8 | Sonia Formation | MWR 14-129 | N 26.400°; E 73.052° | Medium-grained sandstone (quartz-arenite) |
| 9 | Sonia Formation | MWR 14-131,132,133 | N 26.329°; E 73.002° | Medium-grained sandstone (quartz-arenite) |
| 10 | Sonia Formation | MR 14-1 | N 26.553°; E 73.415° | Shale |
| 11 | Sonia Formation | MR 14-2 | N 26.553°; E 73.415° | Coarse-grained sandstone |
| 12 | Sonia Formation | MR 14-13 | N 26.938°; E 71.902° | Shaly sandstone |
| 13 | Sonia Formation | MR 14-15 | N 26.319°; E 72.946° | Medium-grained sandstone (quartz-arenite) |
| 14 | Sonia Formation | MR 14-17 | N 26.305°; E 73.019° | Medium-grained sandstone (quartz-arenite) |
| 15 | Sonia Formation | MWR 15-1 | N 27.123°; E 74.304° | Medium-grained sandstone (quartz-arenite) |
| 16 | Sonia Formation | MWR 15-2 | N 27.163°; E 74.353° | Fine-grained sandstone |
| 17 | Sonia Formation | MWR 15-6 | N 27.163°; E 74.353° | Shale |
| 18 | Girbhakar Formation | MWR 14-128 | N 26.400°; E 73.052° | Gritty sandstone |
| 19 | Girbhakar Formation | MR 14-5 | N 26.222°; E 73.688° | Medium-grained sandstone |
| 20 | Gotan Formation | MWR 14-40 | N 26.667°; E 73.733° | Siliceous limestone |
| 21 | Gotan Formation | MWR 14-66,86,95 | N 26.494°; E 73.800° | Siliceous limestone |
| 22 | Nagaur Formation | MWR 14-13 | N 26.785°; E 73.684° | Gritty calcareous sandstone (arkose) |
| 23 | Nagaur Formation | MWR 14-14 | N 26.785°; E 73.684° | Coarse-grained sandstone (arkosic arenite) |
| 24 | Nagaur Formation | MWR 14-15 | N 26.785°; E 73.684° | Coarse-grained sandstone (arkosic arenite) |
| 25 | Nagaur Formation | MR 14-11 | N 28.402°; E 73.658° | Fine-grained sandstone |
| 26 | Tunklian Formation | MWR 14-45 | N 26.637°; E 73.770° | Shale |
| 25 | Tunklian Formation | MWR 14-46 | N 26.637°; E 73.770° | Medium-grained sandstone (quartz-arenite) |
| 26 | Tunklian Formation | MR 14-8 | N 26.637°; E 73.770° | Medium-grained sandstone (quartz-arenite) |
| | *Basement Rocks* | | | |
| 27 | Malani Igneous Suite | MWR 14-130 | N 26.400°; E 73.052° | Rhyolite |
| 28 | Malani Igneous Suite | MR 14-14 | N 26.594°; E 72.326° | Rhyolite |
| 29 | Malani Igneous Suite | MWR 14-134 | N 26.303°; E 73.025° | Welded Tuff |
| 30 | Erinpura Granites | ERG | N 26.520°; E 73.387° | Granite |
| 31 | Erinpura Granites | Sirohi 14-1 | N 24.874°; E 72.882° | Granite gneiss |
| 32 | Erinpura Granites | Sirohi 14-2 | N 24.874°; E 72.882° | Metagranite |
| 33 | Delhi Supergroup | PH 15-1 | N 25.554°; E 73.861° | Calc silicate |
| 34 | Delhi Supergroup | PH 15-2 | N 25.554°; E 73.861° | Quartzite |
| 35 | Delhi Supergroup | PH 15-45 | N 25.073°; E 73.866° | Quartzite |
| 36 | Delhi Supergroup | PH 15-28 | N 25.759°; E 74.061° | Micaceous quartzite |
| 37 | Delhi Supergroup | PH 15-16 | N 25.624°; E 73.826° | Schist |
| 38 | Delhi Supergroup | PH 15-30 | N 25.775°; E 74.042° | Metapelite |
| 39 | Banded Gneissic Complex-2 | PH 15-34 | N 26.089°; E 74.449° | Biotite granite gneiss |
| 40 | Banded Gneissic Complex-2 | PH 15-36 | N 26.093°; E 74.494° | Granite gneiss |
| 41 | Banded Gneissic Complex-2 | PH 15-37 | N 26.093°; E 74.597° | Granite gneiss |
| 42 | Banded Gneissic Complex-2 | PH 15-38 | N 26.098°; E 74.624° | Granite gneiss |

**Table 2**
Rb-Sr whole rock data for the Chhoti Khatu tuff.

| Sample | Rb (ppm) | Sr (ppm) | $^{87}Rb/^{86}Sr$ | $^{87}Sr/^{86}Sr$ |
|---|---|---|---|---|
| MWR 15-3 | 90.06 | 18.39 | 14.44 | 0.904225 |
| MWR 15-4 | 84.27 | 17.89 | 13.88 | 0.899269 |
| MWR 15-5 | 78.68 | 12.83 | 18.14 | 0.941002 |
| MWR 15-7 | 65.31 | 10.59 | 18.25 | 0.944467 |
| MWR 15-8 | 56.77 | 11.41 | 14.68 | 0.909963 |

Note: Rb and Sr concentrations were measured using Q-ICPMS. External reproducibility for Rb and Sr measurements were < 3% at 2σ level.

protocol for trace elements and HF-$HNO_3$-HCl protocol for Sr-Nd isotopic ratio analyses. Concentrations of trace elements (including REEs) were measured on a Thermo Q-ICPMS using BHVO-2 rock standard (from USGS) as a calibration standard. Machine drift was corrected using In and Bi as internal standards. BHVO-2 was also used as an unknown for accuracy and precision checks. Sr was separated from other elements by means of conventional cation exchange column chromatography and Nd was separated from other REE's by column chemistry using Ln-specific resin from Eichrom with dilute HCl as elutant. $^{87}Sr/^{86}Sr$ and $^{143}Nd/^{144}Nd$ were measured on Isoprobe-T TIMS and Thermo Neptune MC-ICPMS, respectively, in static multi-collection mode. Isotopic ratios were corrected for mass fractionation using $^{86}Sr/^{88}Sr$ ratio of 0.1194 and $^{146}Nd/^{144}Nd$ ratio of 0.7219. The average $^{87}Sr/^{86}Sr$ ratio of NBS987 measured on TIMS over a period of 4 years is 0.71023 ± 1 (2σ, n = 50). The average $^{143}Nd/^{144}Nd$ of the in-house lab standard, Merck Nd solution, was 0.511705 ± 27 (2σ, n = 56). The sample data were normalized using its reported $^{143}Nd/^{144}Nd$ ratio of 0.511734, which is equivalent to La Jolla $^{143}Nd/^{144}Nd$ ratio of 0.511858 (Yang et al., 2011). BHVO-2 yielded $^{143}Nd/^{144}Nd$ ratio of 0.512971 ± 18 (2σ, n = 19), which is within the reported $^{143}Nd/^{144}Nd$ ratio of 0.512979 ± 28 (2σ), (Jochum et al., 2005).

Least altered calcite matrix samples, confirmed by petrography, were microdrilled out of polished slabs/hand specimens of limestone/dolostone samples for isotopic and trace element analyses. Stable C and O isotope ratio analyses of the selected samples were carried out in a Thermo MAT 253 isotope ratio mass spectrometer. $CO_2$ was extracted using Kiel IV Carbonate Device after reaction with 100% orthophosphoric acid at 72 °C. $\delta^{13}C$ and $\delta^{18}O$ were measured in dual inlet mode against a pre-calibrated laboratory standard and converted to V-PDB. External precision was better than ± 0.06‰ (1σ) for $\delta^{13}C$ and ± 0.1‰ (1σ) for $\delta^{18}O$. Ca, Mg, Mn and Sr contents of the carbonate samples were analyzed using Q-ICPMS. Samples were dissolved and diluted using 2% $HNO_3$ and measurements were carried out using COQ-1 (from USGS) as a calibration standard. Machine drift was corrected using Ga and In as internal standards. COQ-1 was also used as an unknown for accuracy and precision checks. For Sr isotopic ratio analysis of limestones, samples were leached using 10% $CH_3COOH$ following the technique prescribed by Ray et al. (2003), and Sr was separated by means of column chromatography using Sr-specific resin from Eichrom with $H_2O$ as elutant. $^{87}Sr/^{86}Sr$ ratio measurements were carried out using Isoprobe-T TIMS in static multi-collection mode as mentioned above.

## 4. Results

### 4.1. Geochronology

Rb-Sr whole rock isotopic ratio and concentration data of the Chhoti Khatu tuff are given in Table 2. The Rb-Sr whole-rock isochron is plotted in Fig. 4, with the linear regression fitted using Isoplot 3.75 (Ludwig, 2012) yielding a date of 703 ± 40 Ma (2σ; MSWD = 2.3). The regression line is not a mixing line because the initial $^{87}Sr/^{86}Sr$ remains constant when plotted against the varying 1/Sr (plot not shown), which suggests that the silicate materials in the tuff was

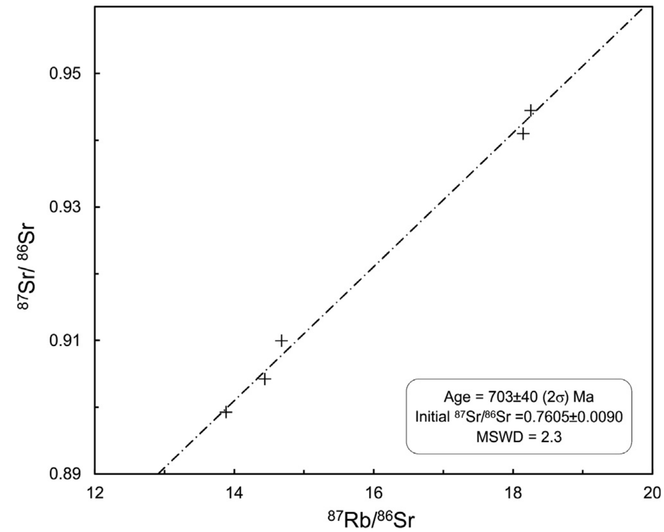


**Fig. 4.** Plot of $^{87}Sr/^{86}Sr$ versus $^{87}Rb/^{86}Sr$ for Chhoti Khatu Tuff using data from Table 2. The isochron and age calculations are done using Isoplot 3.75 (Ludwig, 2012). Uniform errors of 1.5% and 0.001% for $^{87}Rb/^{86}Sr$ and $^{87}Sr/^{86}Sr$, respectively, are used for the isochron.

derived from a (isotopically) homogenized magma. Mixing, if any, could have happened at the source giving a crustal signature to the initial ratio ($^{87}Sr/^{86}Sr_{init}$ = 0.7605). Therefore, the date of 703 Ma can be considered as the age of crystallization of the minerals in the tuff, and hence the age of deposition of the formation. Although, the Rb-Sr dating method is not as robust as the U-Pb zircon dating, the fact that a previous attempt using the latter could only provide a maximum age of ~700 Ma (the age of the youngest recycled zircon; Xu and Meert, 2014) makes our Rb-Sr isochron age significant.

We have utilized Sr isotope stratigraphy to constrain the age of deposition of the Gotan Limestone in the Bilara Group (Fig. 5). Ca, Mn and Sr concentration ratios were used to gauge the extent of alteration of the carbonate fractions analyzed for Sr isotopic ratio (Table 3). Samples with Mn/Sr < 1 and Mg/Ca < 0.1, (Table 3) suggesting least altered nature of their Sr systematics, were selected for Sr isotope stratigraphy. To determine the most pristine $^{87}Sr/^{86}Sr$ of the Gotan Formation that could represent the seawater from which it precipitated, we plotted $^{87}Sr/^{86}Sr$ vs. Ca/Sr (Fig. 5). The plot yielded a linear relationship with the sample showing the lowest $^{87}Sr/^{86}Sr$ also has the highest Sr content and Mn/Sr of 0.14. This ratio (0.708097) can be considered as the best representative of the primordial $^{87}Sr/^{86}Sr$ for the formation and thus the ratio in the coeval seawater. The ratio yielded

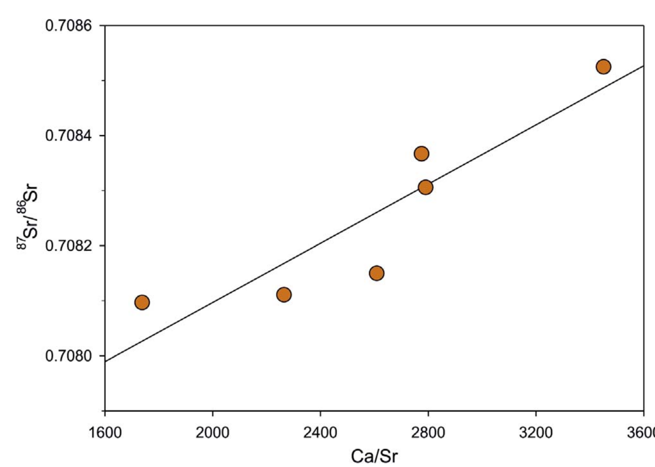


**Fig. 5.** Plot of $^{87}Sr/^{86}Sr$ versus Ca/Sr for samples from the Gotan Limestone. The line represents linear regression (y = 0.7076, $r^2$ = 0.82).

**Table 3**
Isotopic and trace elements data for the Gotan Limestone.

| Sample ID | $\delta^{13}C_{VPDB}$ (‰) | $\delta^{18}O_{VPDB}$ (‰) | Ca/Sr × $10^4$ | Mn/Sr | Mg/Ca | $^{87}Sr/^{86}Sr$ |
|---|---|---|---|---|---|---|
| MWR 14-37 | 0.1 | −0.1 | 0.174 | 0.14 | 0.021 | 0.708097 |
| MWR 14-79 | 0.0 | −0.6 | 0.226 | 0.40 | 0.018 | 0.708111 |
| MWR 14-85 | −1.8 | −5.4 | 0.345 | 0.13 | 0.005 | 0.708525 |
| MWR 14-95 | −1.8 | −5.1 | 0.277 | 0.07 | 0.011 | 0.708367 |
| MWR 14-17 | 0.3 | −3.2 | 0.261 | 0.11 | 0.039 | 0.708150 |
| MWR 14-121 | −0.4 | −5.2 | 0.279 | 0.22 | 0.007 | 0.708306 |

Note: Concentrations were measured using Q-ICPMS. External reproducibility for Ca and other trace elements were < 6% at 2σ level.

two probable ages; an early Cambrian age of 520–530 Ma and a late Ediacaran age of circa 570 Ma, when correlated with the global seawater Sr isotope curve (McArthur et al., 2012). However, the detrital zircon maximum age constraint of 540 Ma placed on the overlying Nagaur Formation (McKenzie et al., 2011) and lack of evidence for any Cambrian fossils in the Gotan Formation hints at a late Ediacaran age (~570 Ma) for the Gotan Formation. It should be noted that this is an approximate age because the method is a relative dating technique and the uncertainty associated with fitting of the seawater evolution curve for $^{87}Sr/^{86}Sr$ from which ages are determined is large.

### 4.2. Trace element geochemistry

Trace element data for siliciclastic sediments of the Marwar Supergroup are presented in Table 4 and are plotted in Fig. 6. In Primitive Mantle (PM) normalized diagram (Fig. 6A) these sediments generally show enrichments in Th, U and Pb and depletions in Nb, Ta, Sr and Eu. They also show LREE enriched patterns in Chondrite normalized plot (Fig. 6B), with the $La_N/Yb_N$ ranging from 4.7 to 27.4. HREE show almost flat patterns (Fig. 6B), with $Gd_N/Yb_N$ falling in a range of 1.0–3.5. A conspicuous negative Eu anomaly is observed in all samples (Fig. 6B) with an average [Eu/Eu*] value of 0.64.

Among the basement rocks we have analyzed (Table 5); the Malani rhyolites show a noticeable depletion in Sr and Eu when compared with the Marwar sedimentary rocks in the PM normalized plot (Fig. 6A). The basement at the eastern parts of the basin, the Erinpura Granites, shows similar patterns as that of the Marwar sediments albeit with depletions in Zr and Hf. All the probable source rocks show LREE enriched Chondrite normalized patterns (not shown). The $La_N/Yb_N$ ranges from 3.5 to 5.3 for the Malani rhyolite and 2.3–10.9 for the Erinpura Granites. The gneiss samples from BGC-2 shows higher values for $La_N/Yb_N$ ratio ranging from 10.4 to 18.1, while rocks from Delhi Supergroup have this ratio in the range of 1.8–16.4. The $Gd_N/Yb_N$ ratio ranges from 1.1 to 1.7 in the Malani rhyolite, 0.9–2.1 in the Erinpura Granites, 1.7–3.9 in the BGC-2 and 1.0–2.9 in the Delhi Supergroup.

### 4.3. Sr-Nd isotope geochemistry

The Sr and Nd isotopic ratio data for all the samples are given in Table 4. The $^{87}Sr/^{86}Sr$ of the sandstone samples from the Jodhpur Group vary in the range of 0.71–0.79 and that of the intercalated shale bands in the range of 0.72–0.87 (Table 4). Nagaur Group rocks display a larger spread in their $^{87}Sr/^{86}Sr$ values: 0.72–0.84. All the samples display predominantly crustal signatures. However, considering that $^{87}Sr/^{86}Sr$ is heavily dependent on grain size variation and susceptible to alteration by secondary processes (e.g., diagenesis and metamorphism) we use it sparingly for our interpretations on the provenances.

The $\varepsilon_{Nd}$ (0) of Marwar siliciclastic sediments vary from −21.8 to −8.5 (Table 4). $\varepsilon_{Nd}$ (0) of the Sonia Sandstone at the contact with basement shows an average value of −9.0, whereas the middle and upper parts of the formation have values in the range of −21.8 to −15.7 and −19.2 to −16.3, respectively. The Girbhakar Formation which forms the top part of the Jodhpur Group has $\varepsilon_{Nd}$ (0) in the range of −21.8 to −20.0. The carbonate sequences of the Bilara Group separate the Jodhpur Group from the overlying Nagaur Group. The $\varepsilon_{Nd}$ (0) of the siliciclastic detritus separated from the Gotan Limestone of the Bilara Group vary in the range of −17.4 to −13.4. Sandstones at the lower part of the Nagaur Formation show $\varepsilon_{Nd}$ (0) of −16.4 to −14.7, whereas that at the top of the Nagaur Formation has a value of −21.6. Sandstone samples from the Tunklian Formation, the topmost lithounit of the Marwar Supergroup, display a range of $\varepsilon_{Nd}$ (0) values from −13.7 to −12.5, while the shale intercalated with the sandstone possesses a much lower value of −20.2. The Marwar sediments have lower radiogenic $\varepsilon_{Nd}$ (0) values compared with that of the basement Malani rhyolites. The rhyolites and associated tuff of MIS display $\varepsilon_{Nd}$ (0) of 0.2 and 6.7, respectively (Table 5). Samples from the potential sediment sources for the Marwar Basin show $\varepsilon_{Nd}$ (0) in the range of −30.0 to −17.3 for the BGC-2, −16.1 to −10.4 for the Erinpura Granites and −17.6 to −11.6 for the Delhi Supergroup.

The $f^{Sm/Nd}$ of the Marwar sediments vary from −0.55 to −0.25; whereas that of the MIS rhyolite and Erinpura Granites varies from −0.33 to −0.29 and −0.40 to −0.12, respectively. Similarly, the $f^{Sm/Nd}$ of the BGC-2 and the Delhi Supergroup rocks varies in similar ranges: from −0.44 to −0.32 and −0.37 to −0.12, respectively (Table 5). The Depleted Mantle model ages ($T_{DM}$) of the Marwar sediments range from 1.2 to 2.8 Ga with a mode at 2.0 Ga. Among the basement rocks, the Malani rhyolites have a narrow range of $T_{DM}$ from 0.9 to 1.0 Ga and the Erinpura Granites show a wide range of $T_{DM}$ from 1.6 to 2.1 Ga. The $T_{DM}$ of BGC-2 varies from 2.6 to 2.9 Ga.

## 5. Discussion

### 5.1. Age constraints on Marwar sedimentation

The very presence of the Chhoti Khatu felsic tuff between Sonia and Girbhakar Formations suggests that the Marwar basin had remained volcanically active even after significant amount of sedimentation, well beyond the last phase of basement volcanism. Based on detrital zircon geochronology, Xu and Meert (2014) had suggested a maximum age of 702 Ma for the deposition of the tuff. This is consistent with the Rb-Sr whole rock isochron age of 703 ± 40 Ma, determined by us. It was generally believed that the sedimentation in the Marwar basin got initiated in the Ediacaran period, ~115 Ma after the Malani magmatism. The lack of physical evidence for Neoproterozoic global glaciations in the Marwar basin was often cited as the rationale behind this argument (see Davis et al., 2014; Turner et al., 2014). However, the new age information suggests that the deposition of the Marwar Supergroup began very much during the Cryogenian period and that the perceived hiatus between the MIS and Marwars may not have been that long after all.

As discussed in Section 4.1, the lowest $^{87}Sr/^{86}Sr$ of 0.708097 displayed by the Gotan Limestone places its deposition time at circa 570 Ma, in the late Ediacaran Period. The carbon isotopic data from these rocks also support this. During the Late Neoproterozoic, $\delta^{13}C$ of the marine carbonates underwent fluctuations and stabilized at ~0‰ subsequent to the Marinoan glaciation and until the next excursion, the Shuram anomaly (Halverson and Shields-Zhou, 2011). $\delta^{13}C$ of the Gotan Limestone shows an average composition of −0.6 ± 1.8 (2σ)‰

**Table 4**
Geochemical data for samples from siliciclastic formations and silicate fractions in limestones of the Marwar Supergroup.

| | Sonia Formation | | | | | | | |
|---|---|---|---|---|---|---|---|---|
| Sample ID | MWR 14-1 | MWR 14-126 | MWR 14-127 | MWR 14-129 | MWR 14-131 | MWR 14-132 | MWR 14-133 | MR 14-1 |
| Sc | 0.54 | 9.9 | 2.0 | 0.53 | 1.3 | 1.3 | 1.2 | 10.72 |
| V | 8.7 | 59 | 24 | 3.1 | 3.8 | 4.6 | 3.4 | 61.92 |
| Cr | 135 | 99 | 217 | 149 | 160 | 187 | 152 | 90 |
| Co | 0.22 | 4.7 | 1.2 | 0.35 | 0.11 | 0.10 | 0.13 | 9.7 |
| Ni | 0.47 | 16.7 | 5.1 | 0.37 | 0.08 | 0.55 | – | 24 |
| Rb | 35 | 136 | 30 | 0.44 | 0.38 | 1.19 | 0.73 | 159 |
| Sr | 21 | 406 | 81 | 25 | 41 | 43 | 48 | 43 |
| Y | 2.24 | 26 | 9.2 | 1.9 | 4.1 | 3.7 | 3.9 | 11.00 |
| Zr | 50 | 212 | 77 | 23 | 51 | 42 | 53 | 127 |
| Nb | 0.83 | 11.4 | 4.8 | 0.46 | 1.9 | 1.5 | 1.7 | 11.8 |
| Cs | 0.59 | 14 | 2.3 | 0.09 | 0.06 | 0.10 | 0.08 | 13.86 |
| Ba | 267 | 250 | 82 | 6.3 | 17 | 30 | 20 | 408 |
| La | 4.1 | 35.7 | 12.6 | 6.0 | 9.1 | 9.3 | 10.8 | 22.4 |
| Ce | 8.1 | 75 | 27.8 | 12.3 | 19.4 | 20.4 | 24.2 | 45 |
| Pr | 0.91 | 8.7 | 2.99 | 1.32 | 2.14 | 2.19 | 2.57 | 5.16 |
| Nd | 3.3 | 32.0 | 11.6 | 4.7 | 7.6 | 7.8 | 8.8 | 18.5 |
| Sm | 0.59 | 6.6 | 2.66 | 0.72 | 1.23 | 1.36 | 1.38 | 3.13 |
| Eu | 0.21 | 1.20 | 0.47 | 0.157 | 0.32 | 0.34 | 0.37 | 0.66 |
| Gd | 0.59 | 6.9 | 2.23 | 0.72 | 1.21 | 1.32 | 1.39 | 3.03 |
| Tb | 0.072 | 0.87 | 0.275 | 0.075 | 0.141 | 0.141 | 0.154 | 0.38 |
| Dy | 0.38 | 4.70 | 1.71 | 0.39 | 0.81 | 0.81 | 0.82 | 2.13 |
| Ho | 0.073 | 0.92 | 0.37 | 0.073 | 0.160 | 0.143 | 0.152 | 0.39 |
| Er | 0.231 | 2.59 | 1.13 | 0.234 | 0.49 | 0.47 | 0.44 | 1.17 |
| Tm | 0.034 | 0.39 | 0.163 | 0.037 | 0.076 | 0.069 | 0.069 | 0.20 |
| Yb | 0.262 | 2.59 | 1.07 | 0.279 | 0.56 | 0.51 | 0.52 | 1.23 |
| Lu | 0.038 | 0.38 | 0.160 | 0.039 | 0.088 | 0.078 | 0.081 | 0.184 |
| Hf | 1.3 | 5.9 | 2.2 | 0.68 | 1.4 | 1.14 | 1.5 | 3.6 |
| Ta | 0.061 | 0.90 | 0.43 | 0.023 | 0.13 | 0.111 | 0.13 | 0.84 |
| Pb | 4.5 | 6.8 | 1.5 | 2.2 | 1.8 | 1.9 | 2.4 | 5.79 |
| Th | 1.9 | 16 | 7.7 | 2.9 | 4.0 | 3.5 | 3.9 | 9.6 |
| U | 0.41 | 2.1 | 0.98 | 0.27 | 0.35 | 0.29 | 0.35 | 1.9 |
| Th/Sc | 3.6 | 1.6 | 3.8 | 5.5 | 3.0 | 2.6 | 3.2 | 0.90 |
| Zr/Sc | 93 | 21 | 39 | 44 | 39 | 32 | 44 | 12 |
| $La_N/Yb_N$ | 11.1 | 9.9 | 8.5 | 15.5 | 11.6 | 13.0 | 14.9 | 13.0 |
| $Gd_N/Yb_N$ | 1.86 | 2.2 | 1.72 | 2.12 | 1.78 | 2.12 | 2.20 | 2.03 |
| $Eu/Eu^*$ | 1.08 | 0.5 | 0.59 | 0.67 | 0.81 | 0.78 | 0.81 | 0.65 |
| $^{143}Nd/^{144}Nd$ | 0.511536 | 0.511816 | 0.511832 | 0.511804 | 0.511776 | 0.511745 | 0.511727 | 0.511681 |
| $\varepsilon_{Nd}$ (0) | −21.5 | −16.0 | −15.7 | −16.3 | −16.8 | −17.4 | −17.8 | −18.7 |
| $f^{Sm/Nd}$ | −0.42 | −0.38 | −0.29 | −0.52 | −0.50 | −0.49 | −0.52 | −0.48 |
| $T_{DM}$ (Ga) | 2.4 | 2.2 | 2.6 | 1.7 | 1.8 | 1.9 | 1.8 | 2.0 |
| $^{87}Sr/^{86}Sr$ | 0.792722 | 0.721773 | 0.721611 | 0.714306 | 0.713373 | 0.714099 | 0.713215 | 0.840507 |

| | Sonia Formation | | | | | | | Girbhakar Formation |
|---|---|---|---|---|---|---|---|---|
| Sample ID | MR 14-2 | MR 14-13 | MR 14-15 | MR 14-17 | MWR 15-1 | MWR 15-2 | MWR 15-6 | MWR 14-128 |
| Sc | 1.0 | 3.9 | 0.70 | 0.42 | 0.58 | 0.88 | 7.2 | 0.96 |
| V | 5.8 | 27 | 5.5 | 5.3 | 5.3 | 10.8 | 64 | 9.4 |
| Cr | 109 | 175 | 144 | 156 | 140 | 252 | 151 | 263 |
| Co | 0.39 | 2.3 | 0.22 | 0.30 | 0.10 | 0.73 | 18.9 | 0.22 |
| Ni | 0.28 | 4.7 | 0.45 | – | 0.67 | 2.8 | 35 | 0.88 |
| Rb | 31 | 90 | 2.8 | 2.1 | 2.1 | 6.1 | 85 | 2.2 |
| Sr | 14 | 40 | 7.1 | 32 | 15 | 9.3 | 18 | 60 |
| Y | 2.4 | 8.5 | 6.9 | 3.0 | 1.6 | 3.1 | 13 | 3.0 |
| Zr | 48 | 108 | 56 | 32 | 76 | 30 | 120 | 64 |
| Nb | 1.7 | 5.5 | 2.0 | 0.76 | 1.8 | 2.2 | 9.6 | 1.8 |
| Cs | 1.2 | 6.4 | 0.24 | 0.13 | 0.08 | 0.33 | 5.8 | 0.05 |
| Ba | 98 | 283 | 17 | 7.3 | 3.9 | 23 | 230 | 20 |
| La | 9.3 | 12.2 | 7.1 | 8.7 | 5.2 | 13.0 | 28.5 | 13.2 |
| Ce | 18.1 | 26.3 | 16.5 | 17.9 | 9.0 | 19.8 | 55 | 25.1 |
| Pr | 2.09 | 2.61 | 1.62 | 1.95 | 1.06 | 2.33 | 4.8 | 2.71 |
| Nd | 7.2 | 9.5 | 5.6 | 6.4 | 3.7 | 8.2 | 14.7 | 9.0 |
| Sm | 1.13 | 1.94 | 1.11 | 0.95 | 0.73 | 1.16 | 2.23 | 1.45 |
| Eu | 0.19 | 0.41 | 0.21 | 0.165 | 0.104 | 0.165 | 0.45 | 0.24 |
| Gd | 1.06 | 1.94 | 1.26 | 0.99 | 0.90 | 1.57 | 3.5 | 1.45 |
| Tb | 0.105 | 0.251 | 0.180 | 0.103 | 0.069 | 0.125 | 0.34 | 0.150 |
| Dy | 0.50 | 1.46 | 1.20 | 0.58 | 0.281 | 0.52 | 1.82 | 0.67 |
| Ho | 0.092 | 0.292 | 0.246 | 0.115 | 0.057 | 0.104 | 0.38 | 0.116 |
| Er | 0.245 | 0.95 | 0.76 | 0.35 | 0.208 | 0.35 | 1.19 | 0.35 |
| Tm | 0.038 | 0.155 | 0.115 | 0.054 | 0.033 | 0.048 | 0.184 | 0.049 |

(continued on next page)

**Table 4** *(continued)*

| Sample ID | Sonia Formation MR 14-2 | MR 14-13 | MR 14-15 | MR 14-17 | MWR 15-1 | MWR 15-2 | MWR 15-6 | Girbhakar Formation MWR 14-128 |
|---|---|---|---|---|---|---|---|---|
| Yb | 0.251 | 1.09 | 0.82 | 0.40 | 0.263 | 0.310 | 1.20 | 0.35 |
| Lu | 0.041 | 0.158 | 0.118 | 0.055 | 0.044 | 0.047 | 0.180 | 0.052 |
| Hf | 1.3 | 2.9 | 1.6 | 0.92 | 1.9 | 0.77 | 2.3 | 1.8 |
| Ta | 0.112 | 0.39 | 0.15 | 0.039 | 0.108 | 0.17 | 0.75 | 0.105 |
| Pb | 1.6 | 4.0 | 2.9 | 1.23 | 1.6 | 1.9 | 11.8 | 2.0 |
| Th | 2.3 | 2.9 | 3.3 | 2.2 | 1.9 | 1.9 | 10.6 | 6.0 |
| U | 0.54 | 0.63 | 0.65 | 0.28 | 0.46 | 0.55 | 3.1 | 0.36 |
| Th/Sc | 2.3 | 0.8 | 4.6 | 5.1 | 3.2 | 2.1 | 1.5 | 6.3 |
| Zr/Sc | 48 | 28 | 80 | 75 | 132 | 34 | 17 | 66 |
| $La_N/Yb_N$ | 26.7 | 8.1 | 6.2 | 15.4 | 14.1 | 30.1 | 17.0 | 27.4 |
| $Gd_N/Yb_N$ | 3.49 | 1.48 | 1.27 | 2.02 | 2.82 | 4.20 | 2.4 | 3.47 |
| $Eu/Eu^*$ | 0.53 | 0.65 | 0.54 | 0.52 | 0.39 | 0.37 | 0.5 | 0.51 |
| $^{143}Nd/^{144}Nd$ | 0.511635 | 0.512203 | 0.511653 | 0.512151 | 0.511546 | 0.511607 | 0.511520 | 0.511613 |
| $\varepsilon_{Nd}$ (0) | −19.6 | −8.5 | −19.2 | −9.5 | −21.3 | −20.1 | −21.8 | −20.0 |
| $f^{Sm/Nd}$ | −0.52 | −0.41 | −0.51 | −0.55 | −0.39 | −0.57 | −0.54 | −0.52 |
| $T_{DM}$ (Ga) | 1.9 | 1.5 | 1.9 | 1.2 | 2.5 | 1.8 | 2.0 | 1.9 |
| $^{87}Sr/^{86}Sr$ | 0.792406 | 0.784703 | 0.712737 | 0.714125 | 0.717261 | 0.738110 | 0.874059 | 0.715586 |

| Sample ID | Girbhakar Formation MR 14-5 | Gotan Formation MWR 14-40 (Silicate) | MWR 14-66 (Silicate) | MWR 14-86 (Silicate) | MWR 14-95 (Silicate) | Nagaur Formation MWR 14-13 | MWR 14-14 | MWR 14-15 |
|---|---|---|---|---|---|---|---|---|
| Sc | 0.97 | 8.1 | 2.3 | 2.3 | 1.15 | 6.0 | 1.4 | 1.4 |
| V | 7.1 | 80 | 63 | 75 | 49 | 19 | 7.8 | 14 |
| Cr | 197 | 261 | 213 | 267 | 226 | 124 | 201 | 99 |
| Co | 0.49 | 6.9 | 1.8 | 5.2 | 1.6 | 2.4 | 0.35 | 0.34 |
| Ni | 1.9 | 32 | 13 | 75 | 16 | 14 | 0.93 | 0.020 |
| Rb | 7.9 | 111 | 22 | 20 | 12.1 | 150 | 7.4 | 0.44 |
| Sr | 14 | 19 | 12.1 | 9.2 | 6.9 | 40 | 5.9 | 83 |
| Y | 2.6 | 6.1 | 2.1 | 3.4 | 0.63 | 8.5 | 13 | 5.4 |
| Zr | 49 | 149 | 53 | 931 | 23 | 75 | 117 | 95 |
| Nb | 1.4 | 13 | 4.1 | 4.3 | 2.3 | 5.1 | 5.4 | 2.2 |
| Cs | 0.58 | 8.3 | 1.9 | 1.4 | 0.84 | 8.3 | 0.65 | 0.04 |
| Ba | 16 | 307 | 86 | 123 | 56 | 457 | 24 | 16 |
| La | 8.8 | 4.2 | 1.17 | 0.64 | 0.22 | 7.7 | 11.0 | 13.2 |
| Ce | 16.4 | 8.9 | 2.61 | 2.46 | 0.44 | 13.6 | 19.7 | 31.1 |
| Pr | 1.97 | 0.98 | 0.26 | 0.148 | 0.046 | 1.43 | 2.04 | 3.6 |
| Nd | 6.9 | 3.7 | 0.98 | 0.64 | 0.17 | 5.1 | 7.2 | 13.6 |
| Sm | 1.20 | 0.79 | 0.23 | 0.152 | 0.036 | 1.14 | 1.52 | 2.03 |
| Eu | 0.158 | 0.29 | 0.081 | 0.078 | 0.028 | 0.38 | 0.26 | 0.37 |
| Gd | 0.99 | 0.96 | 0.27 | 0.19 | 0.048 | 1.23 | 1.83 | 1.82 |
| Tb | 0.094 | 0.133 | 0.043 | 0.043 | 0.0090 | 0.206 | 0.298 | 0.196 |
| Dy | 0.46 | 0.94 | 0.290 | 0.39 | 0.080 | 1.33 | 2.04 | 1.02 |
| Ho | 0.089 | 0.209 | 0.060 | 0.098 | 0.018 | 0.287 | 0.43 | 0.218 |
| Er | 0.269 | 0.68 | 0.187 | 0.35 | 0.061 | 0.87 | 1.31 | 0.67 |
| Tm | 0.037 | 0.120 | 0.032 | 0.064 | 0.0110 | 0.137 | 0.213 | 0.114 |
| Yb | 0.271 | 0.80 | 0.222 | 0.44 | 0.075 | 0.98 | 1.42 | 0.82 |
| Lu | 0.042 | 0.122 | 0.031 | 0.074 | 0.0120 | 0.140 | 0.209 | 0.131 |
| Hf | 1.3 | 3.1 | 0.88 | 15 | 0.42 | 2.1 | 3.4 | 2.6 |
| Ta | 0.070 | 0.94 | 0.32 | 0.31 | 0.16 | 0.42 | 0.44 | 0.18 |
| Pb | 0.58 | 31 | 5.0 | 5.7 | 1.5 | 11.3 | 4.1 | 4.6 |
| Th | 2.7 | 5.8 | 1.3 | 0.88 | 0.38 | 5.2 | 6.3 | 6.7 |
| U | 0.44 | 20 | 6.4 | 11.6 | 4.5 | 0.74 | 1.05 | 0.68 |
| Th/Sc | 2.8 | 0.7 | 0.5 | 0.4 | 0.33 | 0.9 | 4.6 | 4.8 |
| Zr/Sc | 50 | 18 | 23 | 413 | 20 | 13 | 86 | 68 |
| $La_N/Yb_N$ | 23.3 | 3.8 | 3.78 | 1.03 | 2.06 | 5.7 | 5.5 | 11.6 |
| $Gd_N/Yb_N$ | 3.03 | 0.99 | 0.99 | 0.36 | 0.529 | 1.04 | 1.06 | 1.84 |
| $Eu/Eu^*$ | 0.44 | 1.02 | 1.01 | 1.39 | 2.06 | 0.98 | 0.48 | 0.60 |
| $^{143}Nd/^{144}Nd$ | 0.511518 | 0.511746 | 0.511759 | 0.511860 | 0.511949 | 0.511796 | 0.511878 | 0.511886 |
| $\varepsilon_{Nd}$ (0) | −21.8 | −17.4 | −17.1 | −15.2 | −13.4 | −16.4 | −14.8 | −14.7 |
| $f^{Sm/Nd}$ | −0.55 | −0.35 | −0.29 | −0.28 | −0.36 | −0.32 | −0.35 | −0.41 |
| $T_{DM}$ (Ga) | 1.9 | 2.5 | 2.8 | 2.7 | 2.1 | 2.5 | 2.2 | 2.0 |
| $^{87}Sr/^{86}Sr$ | 0.729132 | | | | | 0.813217 | 0.747717 | 0.725610 |

*(continued on next page)*

**Table 4** *(continued)*

| Sample ID | Nagaur Formation MR 14-11 | Tunklian Formation MWR 14-45 | MWR 14-46 | MR 14-8 | BHVO-2 (Measured) | BHVO-2 (Reported Value) |
|---|---|---|---|---|---|---|
| Sc | 3.5 | 3.2 | 1.11 | 1.3 | 32 | 32 |
| V | 21 | 28 | 5.8 | 6.5 | 314 | 317 |
| Cr | 174 | 70 | 182 | 130 | 275 | 280 |
| Co | 0.49 | 2.7 | 0.21 | 1.3 | 45 | 45 |
| Ni | 0.60 | 5.6 | 0.33 | 1.6 | 118 | 119 |
| Rb | 60 | 60 | 4.3 | 4.9 | 9.2 | 9.11 |
| Sr | 25 | 17 | 8.4 | 6.0 | 391 | 396 |
| Y | 16 | 9.4 | 12.0 | 12.3 | 26 | 26 |
| Zr | 196 | 160 | 72 | 86 | 170 | 172 |
| Nb | 5.6 | 8.5 | 2.4 | 3.3 | 18 | 18 |
| Cs | 1.1 | 3.9 | 0.29 | 0.40 | 0.10 | 0.10 |
| Ba | 387 | 186 | 23 | 24 | 130 | 131 |
| La | 12.6 | 19.0 | 9.0 | 9.2 | 15.1 | 15.2 |
| Ce | 24.8 | 37 | 17.6 | 21.3 | 37 | 37.5 |
| Pr | 3.13 | 3.7 | 2.42 | 2.57 | 5.3 | 5.35 |
| Nd | 11.5 | 13.0 | 8.8 | 10.0 | 24.4 | 24.5 |
| Sm | 2.36 | 2.30 | 1.80 | 2.49 | 6.1 | 6.07 |
| Eu | 0.51 | 0.38 | 0.35 | 0.47 | 2.05 | 2.07 |
| Gd | 2.53 | 2.19 | 2.03 | 2.48 | 6.2 | 6.24 |
| Tb | 0.41 | 0.243 | 0.317 | 0.36 | 0.91 | 0.92 |
| Dy | 2.65 | 1.45 | 2.09 | 2.20 | 5.3 | 5.31 |
| Ho | 0.55 | 0.303 | 0.43 | 0.42 | 0.97 | 0.98 |
| Er | 1.67 | 1.04 | 1.31 | 1.25 | 2.53 | 2.54 |
| Tm | 0.257 | 0.169 | 0.202 | 0.181 | 0.32 | 0.33 |
| Yb | 1.819 | 1.229 | 1.392 | 1.309 | 1.99 | 2 |
| Lu | 0.266 | 0.184 | 0.202 | 0.187 | 0.270 | 0.274 |
| Hf | 5.4 | 4.3 | 2.0 | 2.4 | 4.3 | 4.36 |
| Ta | 0.42 | 0.66 | 0.21 | 0.25 | 1.08 | 1.14 |
| Pb | 5.1 | 4.8 | 3.6 | 6.0 | 1.6 | 1.6 |
| Th | 7.4 | 5.9 | 5.1 | 11.5 | 1.19 | 1.22 |
| U | 1.7 | 1.5 | 0.74 | 0.96 | 0.40 | 0.403 |
| Th/Sc | 2.1 | 1.8 | 4.6 | 8.8 | | |
| Zr/Sc | 55 | 50 | 65 | 66 | | |
| $La_N/Yb_N$ | 5.0 | 11.1 | 4.7 | 5.1 | | |
| $Gd_N/Yb_N$ | 1.15 | 1.48 | 1.20 | 1.57 | | |
| Eu/Eu* | 0.64 | 0.52 | 0.55 | 0.58 | | |
| $^{143}Nd/^{144}Nd$ | 0.511530 | 0.511604 | 0.511998 | 0.511935 | 0.512971 (n = 19) | 0.512979 |
| $\varepsilon_{Nd}$ (0) | −21.6 | −20.2 | −12.5 | −13.7 | | |
| $f^{Sm/Nd}$ | −0.38 | −0.45 | −0.34 | −0.25 | | |
| $T_{DM}$ (Ga) | 2.6 | 2.2 | 2.0 | 2.7 | | |
| $^{87}Sr/^{86}Sr$ | 0.809584 | 0.844489 | 0.733829 | 0.737797 | 0.703471 (n = 3) | 0.703478 |

Note: Concentrations are in ppm. External reproducibility of trace element contents is < 8% and that of REE's is < 3% at 2σ level based on the repeated analysis of BHVO-2. Reported Values for BHVO-2 are from Jochum et al. (2005). Subscript N indicates concentrations are normalized with Chondritic values. $Eu/Eu^* = Eu_N/(Sm_N \times Gd_N)^{0.5}$. $\varepsilon_{Nd}$ (0) was calculated using present day CI Chondritic value of $^{143}Nd/^{144}Nd = 0.512638$. $f^{Sm/Nd}$ is calculated using present day CHUR value of $^{147}Sm/^{144}Nd = 0.1967$. Depleted Mantle Nd model age ($T_{DM}$) is calculated using Depleted Mantle reservoir ratios of $^{143}Nd/^{144}Nd = 0.51315$ and $^{147}Sm/^{144}Nd = 0.2137$.

thereby supporting its Late Neoproterozoic age (Table 3). The newly determined ages of the Chhoti Khatu tuff and Gotan Limestone suggest that either there were protracted depositions of the Girbhakar and Dhanapa Formations or there exists a depositional hiatus between the Jodhpur and Bilara Groups. Since the Sonia and Girbhakar Formations are largely fluvial sandstones a protracted deposition of the Girbhakar is unlikely and therefore, we believe that there may have been a cessation in deposition for about 100 Ma after the deposition of the Jodhpur Group.

### *5.2. Provenance of the Marwar sediments*

The trace elemental patterns of siliciclastic sediments of the Marwar Supergroup are akin to average upper continental crust with typical enrichments in Th, U and Pb and depletions in Nb, Ta and Sr albeit the fact that their overall contents have been lowered as a result of dilution by presence of significant amount of quartz (Fig. 6). There is a significant enrichment in the LREE [$La_N/Yb_N$ = 4.7–27.4] and a very high Th/Sc ratio (0.88–8.80); all indicative of predominance of felsic igneous rocks in the provenance (Fig. 6B, Fig. 7A). The Th/Sc vs Zr/Sc plot (Fig. 7A) shows a minor enrichment in the Zr concentration away from the compositional variation line, which suggests that there had been heavy mineral addition into the sediments due to recycling. These sediments also exhibit a large diversity in Sm/Nd ratio (represented as $f^{Sm/Nd}$) reflecting their derivation from less differentiated sources and poor mixing prior to deposition (McLennan and Hemming, 1992). In addition, there is a large variation in $\varepsilon_{Nd}$ (650 Ma) (Fig. 8) and $T_{DM}$ ages (Fig. 9) of the Marwar sediments which suggests that multiple sources of varying ages contributed detritus to the basin. Marwar sediments display a continental crustal character (Fig. 7A and B); however the overlapping nature of their Nd isotopic ratios with that of the Archean and Paleoproterozoic rocks in the vicinity suggests that these sediments were derived from local sources. The paleocurrent analyses (Awasthi and Parkash, 1981; Chauhan et al., 2004, 2001) in the Sonia and Girbhakar Formations support such an inference by suggesting paleoflow directions from west-southwest, therefore implying that the sources were located along the eastern fringes of the basin.

The central and northwestern part of the basin is largely developed over the MIS, which includes bimodal volcanics dominated by rhyolite and minor exposures of granites. Since the MIS forms the basement in

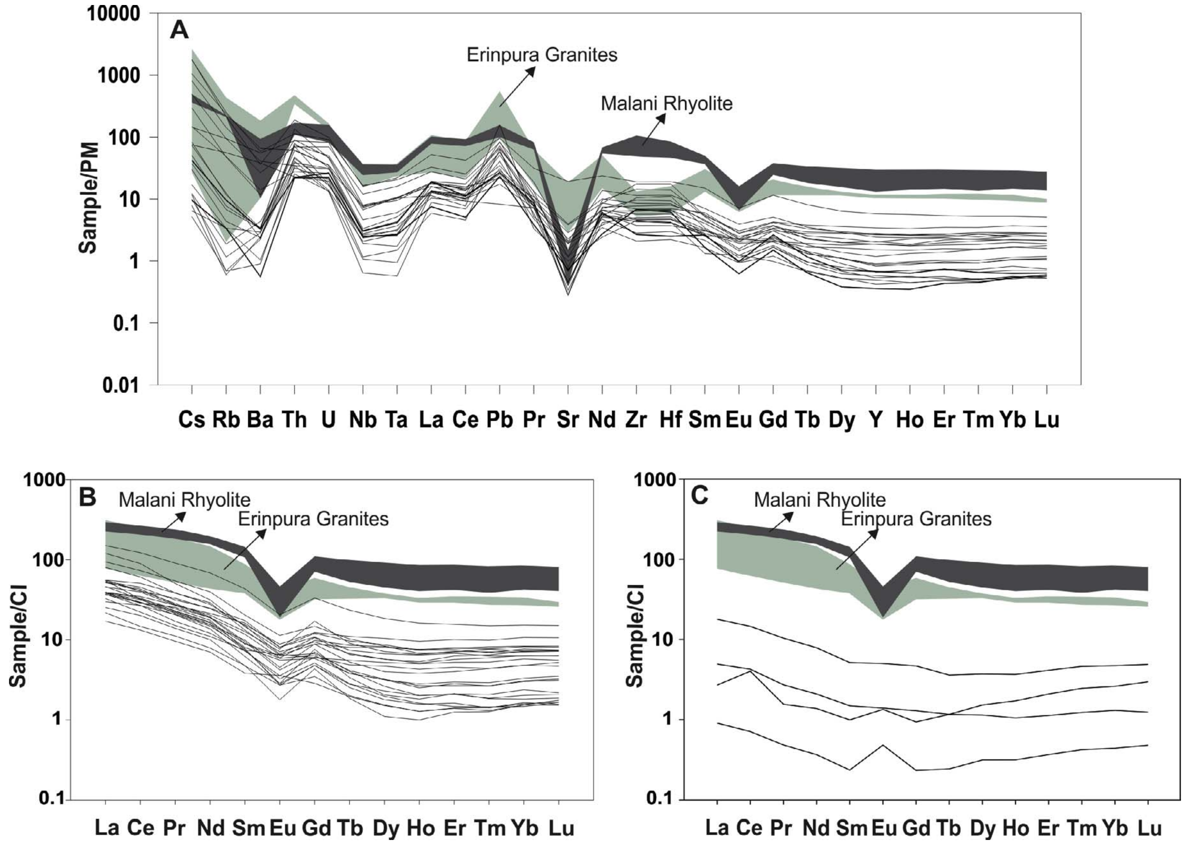


**Fig. 6.** Primitive Mantle normalized multi-element (A) and Chondrite normalized rare earth element (REE) (B) patterns for samples from the siliciclastic formations of the Marwar Supergroup. (C) Chondrite normalized REE patterns for silicate fractions of the samples from the Gotan Limestone. Patterns for basement rocks (MIS rhyolites and Erinpura Granites) are given for comparison. The CI Chondrite and Primitive Mantle values are from Sun and McDonough (1989).

**Table 5**
Geochemical data of representative samples from the basement rocks.

| | Malani Igneous Suite | | | Erinpura Granites | | | Delhi Supergroup | |
|---|---|---|---|---|---|---|---|---|
| Sample ID | MWR 14-130 | MR 14-14 | MWR 14-134 | ERG | Sirohi 14-1 | Sirohi 14-2 | PH 15-1 | PH 15-2 |
| Sc | 1.01 | 8.4 | 1.12 | 9.1 | 13 | 8.6 | 6.0 | 3.8 |
| V | 5.2 | 3.5 | 2.2 | 20 | 70 | 15 | 41 | 3.9 |
| Cr | 166 | 67 | 158 | 188 | 292 | 300 | 79 | 98 |
| Co | 1.17 | 0.67 | 0.69 | 4.4 | 12.0 | 0.65 | 8.7 | 0.76 |
| Ni | 3.9 | 1.06 | 2.5 | 7.2 | 21 | 5.1 | 25 | 1.5 |
| Rb | 142 | 133 | 188 | 214 | 277 | 1.3 | 0.71 | 85 |
| Sr | 8.4 | 31 | 6.3 | 135 | 60 | 388 | 131 | 46 |
| Y | 135 | 59 | 159 | 51 | 46 | 53 | 22 | 2.1 |
| Zr | 1187 | 540 | 1263 | 149 | 85 | 58 | 90 | 22 |
| Nb | 26 | 17 | 27 | 17 | 19 | 11.2 | 7.6 | 10.8 |
| Cs | 2.8 | 4.0 | 7.9 | 4.7 | 21 | 0.21 | 0.089 | 6.4 |
| Ba | 71 | 653 | 139 | 1288 | 396 | 72 | 8.1 | 37 |
| La | 70 | 53 | 23.1 | 74 | 63 | 18.4 | 5.4 | 4.2 |
| Ce | 164 | 126 | 145 | 155 | 132 | 39 | 17.8 | 7.1 |
| Pr | 22.8 | 17.4 | 8.8 | 18.2 | 14.6 | 4.9 | 2.83 | 0.74 |
| Nd | 92 | 73 | 42 | 69 | 53 | 20.3 | 12.4 | 2.32 |
| Sm | 22.2 | 16.3 | 18.5 | 13.5 | 10.5 | 5.8 | 3.24 | 0.48 |
| Eu | 1.10 | 2.69 | 1.08 | 2.54 | 1.238 | 1.036 | 0.75 | 0.260 |
| Gd | 22.7 | 14.6 | 21.1 | 12.2 | 10.5 | 6.6 | 3.4 | 0.44 |
| Tb | 3.6 | 1.96 | 3.8 | 1.67 | 1.44 | 1.21 | 0.57 | 0.064 |
| Dy | 23.4 | 11.4 | 25.9 | 9.6 | 8.4 | 8.4 | 3.6 | 0.36 |
| Ho | 4.9 | 2.31 | 5.4 | 1.81 | 1.67 | 1.90 | 0.74 | 0.070 |
| Er | 14.4 | 7.0 | 16.1 | 5.2 | 4.9 | 5.8 | 2.11 | 0.231 |
| Tm | 2.16 | 1.00 | 2.42 | 0.75 | 0.71 | 0.90 | 0.315 | 0.044 |
| Yb | 14.5 | 7.2 | 16.0 | 4.9 | 4.6 | 5.8 | 2.09 | 0.36 |
| Lu | 2.04 | 1.02 | 2.32 | 0.69 | 0.65 | 0.74 | 0.304 | 0.059 |
| Hf | 26 | 14 | 29 | 5.0 | 2.4 | 1.7 | 2.6 | 0.79 |
| Ta | 1.5 | 1.10 | 1.6 | 1.3 | 1.5 | 0.96 | 0.64 | 1.00 |

(continued on next page)

**Table 5** *(continued)*

| | Malani Igneous Suite | | | Erinpura Granites | | | Delhi Supergroup | |
|---|---|---|---|---|---|---|---|---|
| Sample ID | MWR 14-130 | MR 14-14 | MWR 14-134 | ERG | Sirohi 14-1 | Sirohi 14-2 | PH 15-1 | PH 15-2 |
| Pb | 7.0 | 11.1 | 10.4 | 39 | 23 | 7.0 | 4.2 | 23 |
| Th | 14 | 9.2 | 15 | 32 | 40 | 29 | 3.4 | 1.5 |
| U | 3.3 | 1.7 | 3.0 | 3.5 | 2.7 | 3.5 | 2.0 | 0.39 |
| $Gd_N/Yb_N$ | 1.3 | 1.7 | 1.1 | 2.1 | 1.9 | 0.9 | 1.4 | 1.03 |
| $^{143}Nd/^{144}Nd$ | 0.512637 | 0.512654 | 0.512984 | 0.512104 | 0.511813 | 0.512060 | 0.512046 | 0.511899 |
| $\varepsilon_{Nd}$ (0) | 0.0 | 0.3 | 6.7 | −10.4 | −16.1 | −11.3 | −11.6 | −14.4 |
| $f^{Sm/Nd}$ | −0.29 | −0.33 | | −0.40 | −0.40 | | −0.20 | −0.37 |
| $T_{DM}$ (Ga) | 1.0 | 0.9 | | 1.6 | 2.1 | | 2.9 | 2.1 |
| $^{87}Sr/^{86}Sr$ | 1.158436 | 0.808594 | 1.367432 | 0.760482 | 0.856725 | 0.720317 | 0.718082 | 0.797128 |

| | Delhi Supergroup | | | | BGC-2 | | | |
|---|---|---|---|---|---|---|---|---|
| Sample ID | PH 15-45 | PH 15-28 | PH 15-16 | PH 15-30 | PH 15-34 | PH 15-36 | PH 15-37 | PH 15-38 |
| Sc | 12.1 | 3.2 | 14 | 14 | 15 | 2.0 | 4.9 | 14 |
| V | 21 | 0.82 | 80 | 76 | 84 | 8.2 | 24 | 49 |
| Cr | 40 | 44 | 185 | 235 | 147 | 91 | 117 | 106 |
| Co | 3.6 | 0.009 | 17 | 9.3 | 13 | 5.6 | 5.2 | 7.4 |
| Ni | 6.7 | 1.3 | 32 | 10.9 | 13 | 5.3 | 7.2 | 10.5 |
| Rb | 3.2 | 280 | 126 | 117 | 150 | 93 | 106 | 82 |
| Sr | 32 | 97 | 58 | 19 | 199 | 223 | 193 | 113 |
| Y | 3.7 | 0.041 | 21 | 25 | 58 | 3.6 | 19 | 44 |
| Zr | 11.1 | 0.18 | 122 | 96 | 9.8 | 29 | 187 | 66 |
| Nb | 2.2 | 0.06 | 16.7 | 17.8 | 22.7 | 2.5 | 6.1 | 14 |
| Cs | 0.26 | 11.2 | 5.4 | 4.4 | 0.92 | 0.73 | 1.09 | 1.16 |
| Ba | 9.4 | 331 | 514 | 354 | 1103 | 2832 | 509 | 422 |
| La | 1.16 | 0.225 | 48 | 51 | 115 | 5.8 | 37 | 87 |
| Ce | 3.06 | 0.129 | 102 | 110 | 243 | 8.2 | 88 | 164 |
| Pr | 0.39 | 0.018 | 11.6 | 12.2 | 28.3 | 1.23 | 9.7 | 18.8 |
| Nd | 1.66 | 0.056 | 42 | 45 | 107 | 4.5 | 36 | 67 |
| Sm | 0.47 | 0.0126 | 7.9 | 8.5 | 19.3 | 0.83 | 8.0 | 12.2 |
| Eu | 0.130 | 0.61 | 1.54 | 0.97 | 2.70 | 0.84 | 1.38 | 1.90 |
| Gd | 0.52 | 0.0106 | 7.5 | 7.8 | 17.8 | 0.81 | 7.2 | 12.1 |
| Tb | 0.093 | 0.00082 | 0.90 | 0.98 | 2.24 | 0.098 | 0.86 | 1.56 |
| Dy | 0.61 | 0.0074 | 4.6 | 5.3 | 11.8 | 0.53 | 4.1 | 8.8 |
| Ho | 0.124 | 0.00043 | 0.80 | 1.02 | 2.18 | 0.113 | 0.68 | 1.649 |
| Er | 0.35 | 0.0024 | 2.20 | 3.11 | 5.8 | 0.34 | 1.77 | 4.5 |
| Tm | 0.053 | 0.00049 | 0.312 | 0.50 | 0.75 | 0.052 | 0.236 | 0.62 |
| Yb | 0.37 | 0.0036 | 2.11 | 3.7 | 4.5 | 0.40 | 1.52 | 3.8 |
| Lu | 0.052 | 0.00037 | 0.308 | 0.56 | 0.61 | 0.070 | 0.220 | 0.52 |
| Hf | 0.32 | 0.0057 | 3.3 | 2.6 | 0.44 | 1.07 | 5.5 | 2.3 |
| Ta | 0.64 | 0.033 | 1.09 | 1.3 | 1.02 | 0.60 | 0.51 | 1.01 |
| Pb | 1.3 | 110 | 16 | 7.0 | 24 | 11.8 | 36 | 18 |
| Th | 0.21 | – | 23 | 26 | 20 | 14 | 25 | 28 |
| U | 0.26 | 0.056 | 2.1 | 3.1 | 1.5 | 6.5 | 2.1 | 1.7 |
| $Gd_N/Yb_N$ | 1.17 | 2.46 | 2.9 | 1.7 | 3.2 | 1.68 | 3.9 | 2.6 |
| $^{143}Nd/^{144}Nd$ | 0.511737 | | 0.511834 | 0.511764 | 0.511229 | 0.511100 | 0.511749 | 0.511333 |
| $\varepsilon_{Nd}$ (0) | −17.6 | | −15.7 | −17.1 | −27.5 | −30.0 | −17.3 | −25.5 |
| $f^{Sm/Nd}$ | −0.14 | | −0.12 | −0.18 | −0.44 | −0.44 | −0.32 | −0.44 |
| $T_{DM}$ (Ga) | | | | | 2.7 | 2.9 | 2.6 | 2.6 |
| $^{87}Sr/^{86}Sr$ | 0.729322 | 0.826255 | 0.798371 | 0.899851 | 0.758792 | 0.736112 | 0.753648 | 0.776734 |

Note: Experimental details as described in Table 4.

most parts of the basin, the rhyolites are expected to be the major contributor to the sediments. However, there exists a large disparity of $T_{DM}$ distribution and Nd isotopic composition between the Marwars and the MIS [($\varepsilon_{Nd}$ (650 Ma) = −15.4 to −0.5, $T_{DM}$ = 1.2–2.8 Ga), ($\varepsilon_{Nd}$ (650 Ma) = 3.4–6.2, $T_{DM}$ = 0.9–1.5 Ga)] (Figs. 8 and 9). All the younger $T_{DM}$ ages (1.2–1.7 Ga) and higher $\varepsilon_{Nd}$ (650 Ma) values are reported from the samples collected at the contact between the Malani rhyolite and Sonia Formation suggest that the basement's influence, if any, was limited only to the sediments deposited immediately above it. The Erinpura Granites form the basement in the eastern parts of the Marwar basin. Their $\varepsilon_{Nd}$ (650 Ma) and $T_{DM}$ clearly overlap with that of the Marwars (Figs. 8 and 9), which when considered along with the results of paleocurrent analysis (east to west) suggests that these Granites have been a major source for the Marwar sediments. Rocks of the Delhi Supergroup also show overlapping $\varepsilon_{Nd}$ and $T_{DM}$ with that of the Marwars (Figs. 8 and 9); however, together with the Erinpura Granites these sources cannot explain the entire observed ranges of the Marwar sediments. As suggested by $\varepsilon_{Nd}$ (0) vs. Th/Sc and $f^{Sm/Nd}$ vs. $\varepsilon_{Nd}$ (0) plots (Fig. 7), another major Paleoproterozoic source is required to explain the high $T_{DM}$ values and $\varepsilon_{Nd}$ (650 Ma) values in the Marwars. The BGC-2 fits into this description (Fig. 9) and its very presence at the eastern margin of the basin (Fig. 1) could have made it a major provenance for the Marwar sediments during the Neoproterozoic.

We have made an attempt to quantify the relative contributions of various sources to the Marwar Basin using $\varepsilon_{Nd}$ and Gd/Yb. The latter is chosen since the middle and heavy REE's are known to be resistant to weathering and alteration. $\varepsilon_{Nd}$ was corrected to time of deposition of the Jodhpur, Bilara and Nagpur Groups and Gd/Yb were Chondrite normalized. Ternary mixing curves have been generated assuming the MIS, BGC-2 and Delhi Supergroup/Erinpura Granites as three end-

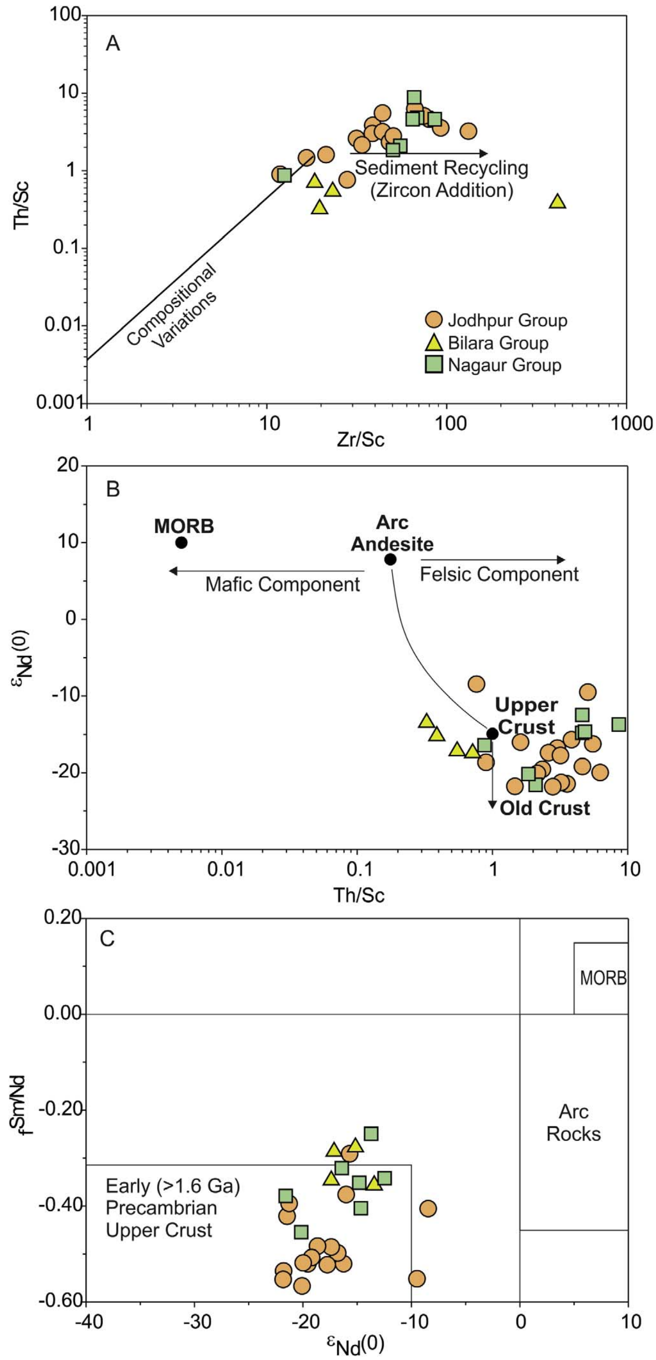


**Fig. 7.** Plots of Th/Sc vs. Zr/Sc (A), $\varepsilon_{Nd}$ (0) vs. Th/Sc (B) and $f^{Sm/Nd}$ vs. $\varepsilon_{Nd}$ (0) (C) for samples from siliciclastic formations of the Marwar Supergroup.

member components in the $\varepsilon_{Nd}$ (T) vs. $Gd_N/Yb_N$ plots (Fig. 10). Three separate plots have been used for the three Groups of Marwar Supergroup (Fig. 10). From the three component mixing plots in Fig. 10, we make the following observations: (1) In spite of its close proximity, the MIS had very limited, if any, contribution to the sediment budget of the entire Marwars; except for at the depositional sites very near to the contact of the topmost MIS and bottommost Marwars (Sample 13, 17 in Fig. 10A); (2) Rocks of the Delhi Supergroup had remained a constant source of sediments (> 30% of the total budget) to the Marwar Basin throughout its depositional history, including the time when fluvial activity was at its lowest, i.e. during the deposition of the Gotan Limestone Formation (Fig. 10B); (3) Contributions of the Erinpura Granites were probably limited to the Jodhpur Group, however, it is

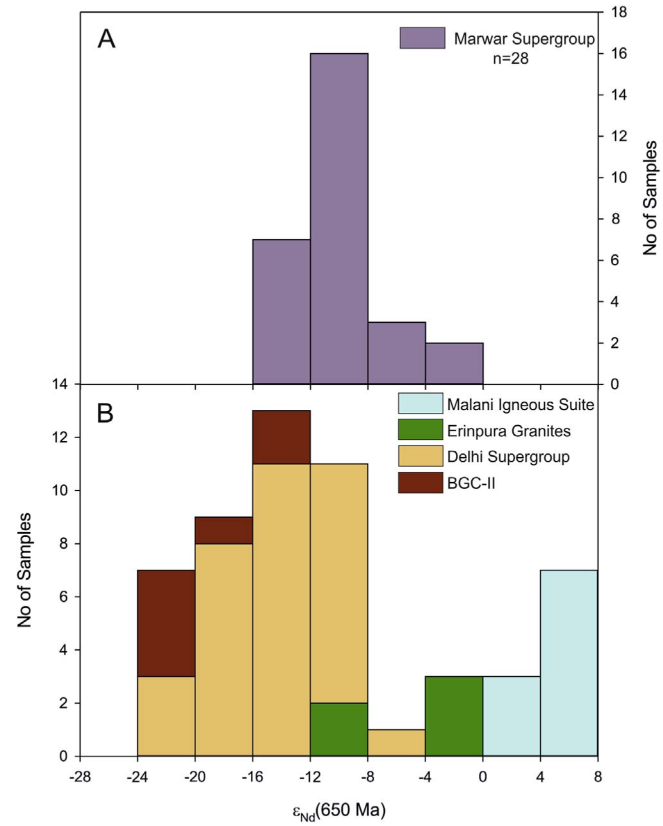


**Fig. 8.** (A) Histogram of $\varepsilon_{Nd}$ (650 Ma) distribution for the Marwar Supergroup, (B) $\varepsilon_{Nd}$ (650 Ma) distribution for the potential sources in a stacked histogram. MIS rhyolite, Erinpura Granites, Delhi Supergroup and BGC-2 data are from Carter (2005), Kaur et al. (2007, 2009, 2011a), Tobisch et al. (1994), Van Lente et al. (2009) and this study (Table 5).

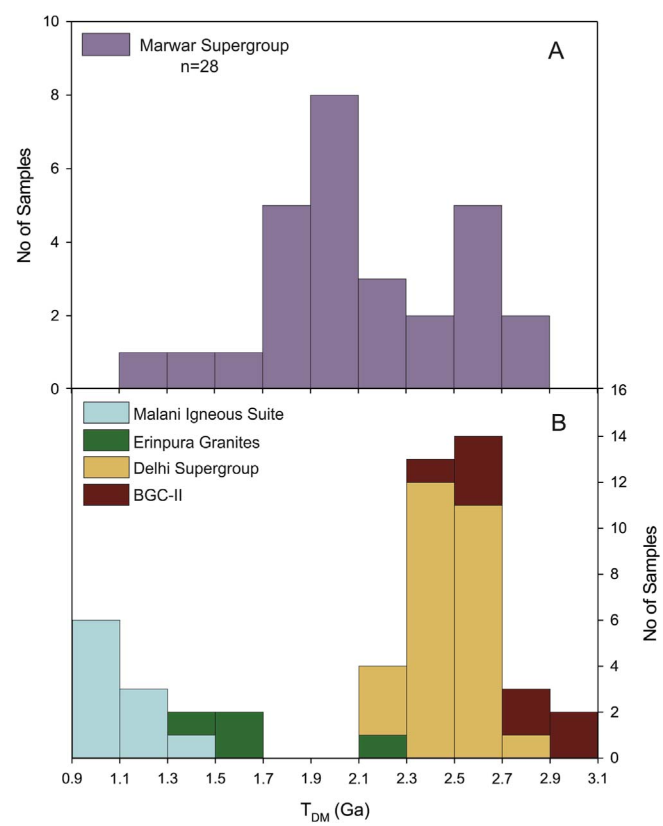


**Fig. 9.** (A) Histogram of $T_{DM}$ distribution for the Marwar Supergroup. (B) Stacked histogram of $T_{DM}$ distribution for the potential sources. Data sources as in Fig. 8.

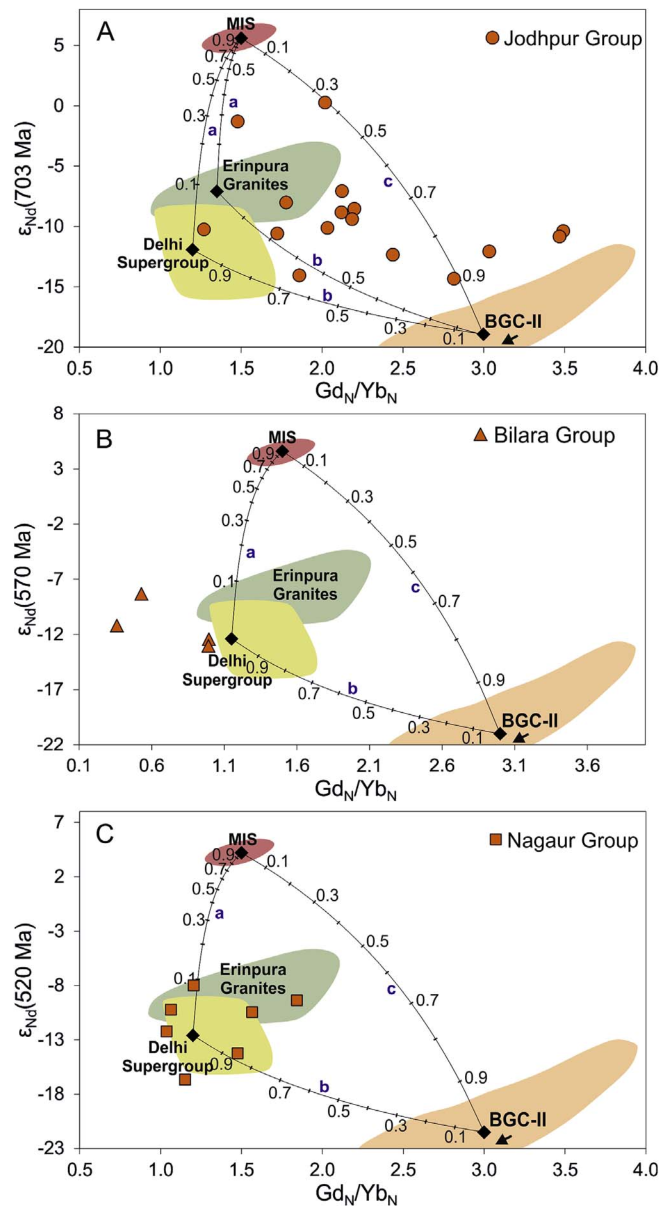


**Fig. 10.** Plot of $\varepsilon_{Nd}$ (T) vs. $Gd_N/Yb_N$ for Marwar siliciclastics in the (A) Jodhpur Group, (B) Bilara Group, and (C) Nagaur Group. Mixing curves are generated with MIS, Delhi Supergroup/Erinpura Granites and BGC-2 as end members. Mixing curves a, b, and c, are drawn for Nd/Yb ratios of 0.25, 2, and 2, respectively, for all the three plots. Data sources: as in Fig. 8.

difficult to rule out complete absence of sediments derived from these, in the younger Groups; (4) The BGC-2 was one of the major sources of sediments to the Jodhpur Group (up to 70% of the total budget), however, its contribution to the basin appears to have ceased subsequent to the deposition of the Girbhakar Formation; (5) While the fluvial activity was virtually non-existent during the deposition of carbonates of the Bilara Group, some amount of siliciclastics did make it into the basin. The composition of these sediments (Fig. 10B) suggests that these were rich in heavy minerals (e.g., garnet) and were primarily derived from the Delhi Supergroup.

The variations of $^{87}Sr/^{86}Sr$ in the Marwar siliciclastics (Fig. 11) appear to suggest that very little recycling of sediments had happened from the Jodhpur Group into the Nagaur Group. Although it is difficult to compare the present day $^{87}Sr/^{86}Sr$ of the sediments with that of the potential sources, because of the differential weathering of minerals in the sources, it is quite clear that the sediments in the Jodhpur Group

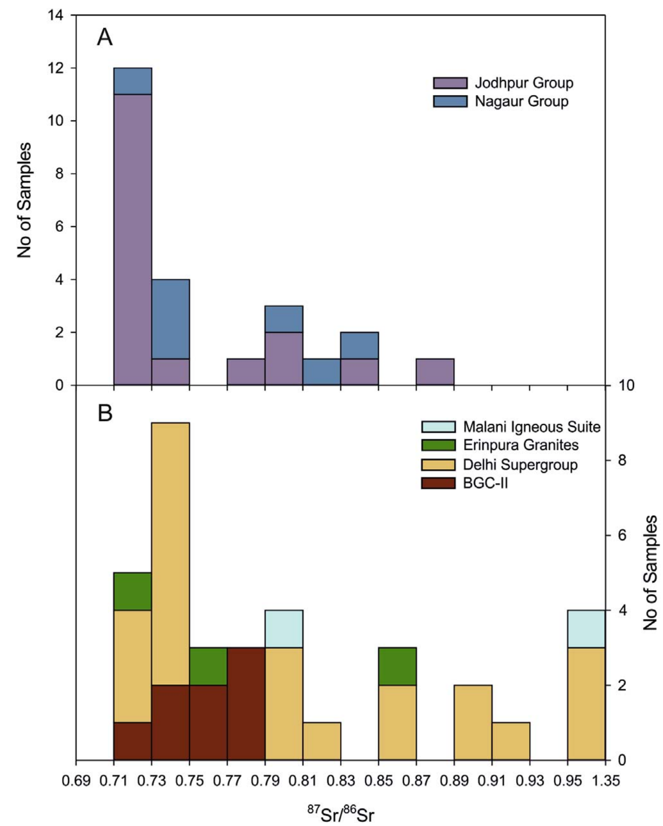


**Fig. 11.** Stacked histogram of $^{87}Sr/^{86}Sr$ for the Jodhpur and Nagaur Groups (A) compared with $^{87}Sr/^{86}Sr$ of potential source regions (B). Data sources: as in Fig. 8.

have a strong signal of being derived from the Delhi Supergroup and the BGC-2 (Fig. 11). The $^{87}Sr/^{86}Sr$ of the Nagaur sediments appears to have a signal of mixed sources (Fig. 11).

### *5.3. Evolution of the Marwar basin and global correlations*

The Rb-Sr whole rock isochron age of 703 ± 40 Ma obtained for the Chhoti Khatu tuff indicates that the sedimentation in the Marwar Basin began shortly after the Malani magmatism. The sedimentation started in the Cryogenian, and not in the Ediacaran Period, as believed earlier. Our provenance study suggests that the Delhi Supergroup, BGC-2 and possibly the Erinpura Granites acted as the major sediment sources to the Jodhpur Group. Various trace element ratios and Nd isotopic composition capture the change in mineralogy of the provenance over the course of the sedimentation (Fig. 12). The $f^{Sm/Nd}$ decreases and $Gd_N/Yb_N$ increases stratigraphically upward in the Jodhpur Group (Fig. 12), which suggest dominance of contributions from Early Precambrian crustal rocks, in this case the BGC-2. The decrease in $\varepsilon_{Nd}$ (0) from bottom to top (from −9 to −21) within the formation supports the above inference. This information, results of paleocurrent analysis, and the predominantly fluvial nature of the sediments clearly suggest that the sediments in the Jodhpur Group were derived from the Aravalli Mountain Ranges which incorporated all the above mentioned lithologies, got deposited on the Erinpura Granites in the eastern fringes of the basin and covered the MIS in the central and western parts of the basin (Fig. 13). This also explains the lack of contribution of MIS to the Marwar sedimentation beyond a few beds at the basement-cover contact. It appears that the topography of the area had already attained almost the current configuration by the time the development of the basin had begun. However, the basin remained volcanically active as suggested by the Chhoti Khatu felsic tuff, which marks the end of sedimentation in the Sonia Formation. The deposition of the tuff was followed by a change in facies from the marginal marine realms of the

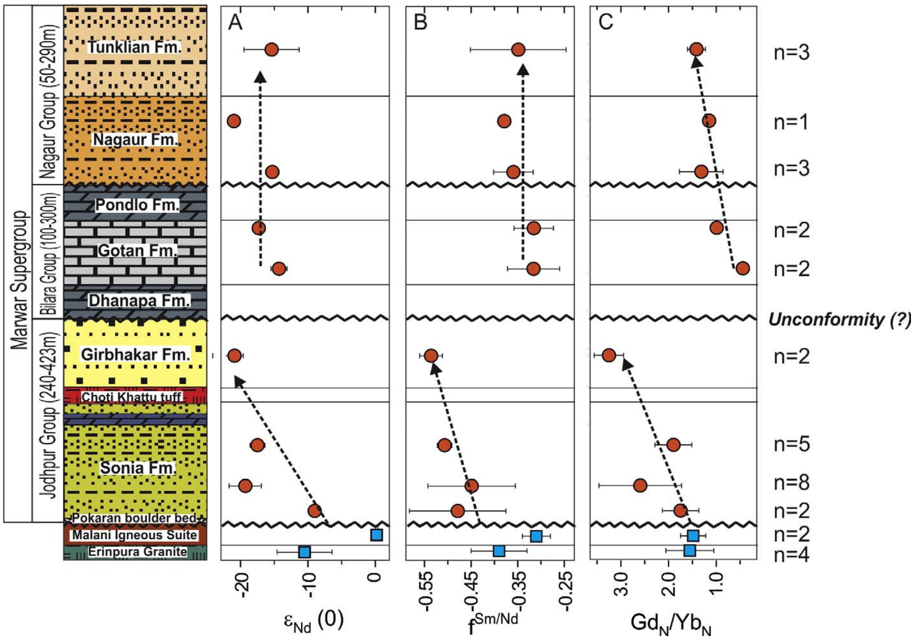


**Fig. 12.** Variations of $\varepsilon_{Nd}$ (0), $f^{Sm/Nd}$ and $Gd_N/Yb_N$ with stratigraphy in the Marwar Supergroup. Error bars are 1σ.

upper Sonia Formation to a more coarse and pebbly sandstone in form of the Girbhakar Formation, which is a braided fluvial deposit. The new age constraints given by us, the paleomagnetic data (Davis et al., 2014) and age distribution of detrital zircons (McKenzie et al., 2011; Turner et al., 2014) allow us to correlate the evolution of the Marwar basin with a host of terminal Neoproterozoic-Early Cambrian basins worldwide, developed along similar equatorial paleolatitudes (Fig. 14). The Jodhpur Group could have evolved contemporaneously with the Arkahawl Formation of the Huqf Supergroup, the Nagthat Formation (Juansar-Simla Groups) of Lesser Himalayas and the Wukiangxi Formation (Liantuo Formation-Banxi Group) of South China; all of which are dominated by both fluvial and shallow marine sandstones, and siltstones (Jiang et al., 2003; Rieu et al., 2007 and the references therein). There is no equivalent succession developed in the Salt Range

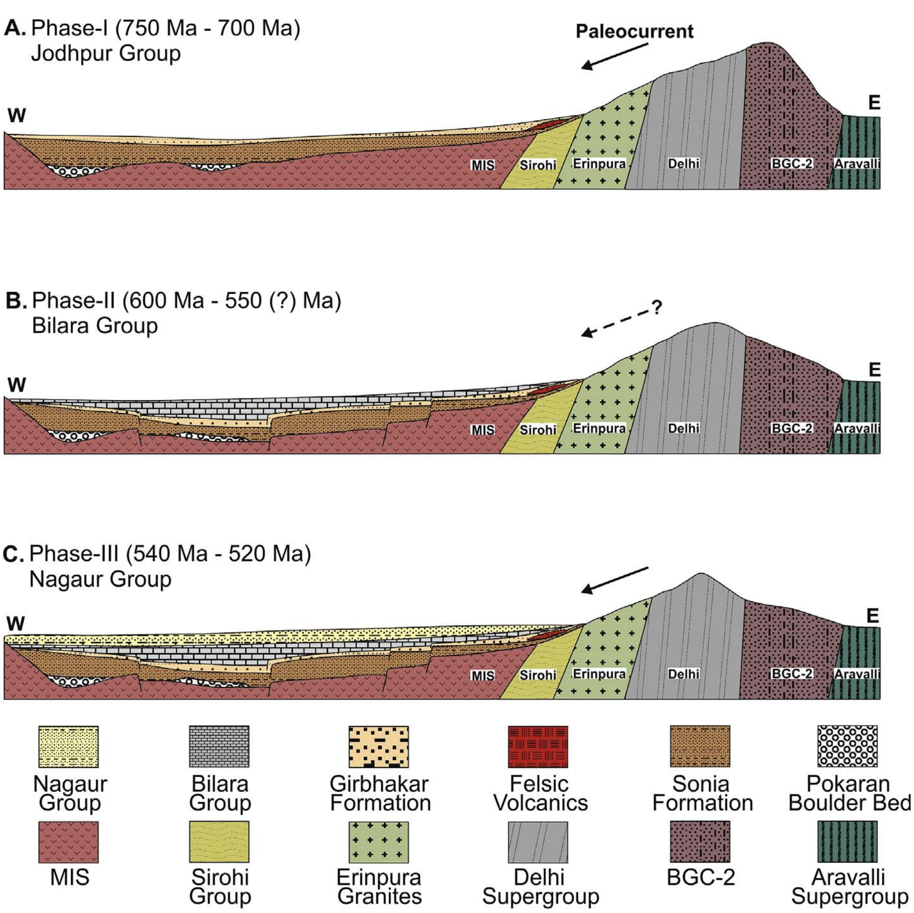


**Fig. 13.** Proposed model for the evolution of the Marwar Basin in three phases. See text for discussion.

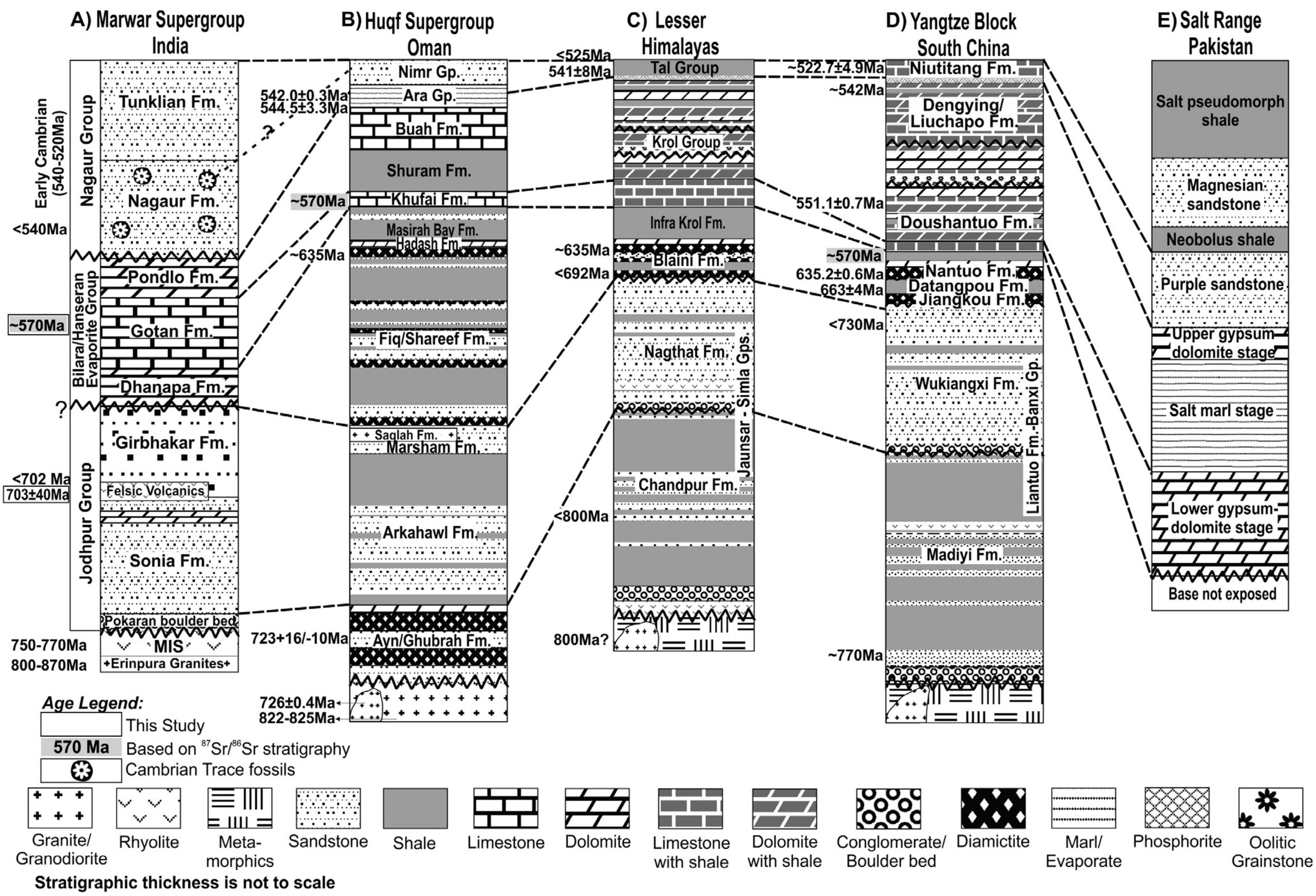


**Fig. 14.** Comparative stratigraphy and proposed correlations between the Marwar Supergroup, the Huqf Supergroup of Oman, the Salt Range of Pakistan, the Lesser Himalayas and the Yangtze platform sequences of India and South China, respectively. The stratigraphic thicknesses are not to scale. Correlations are made mostly based on the available age data, similarity in detrital zircon distribution and paleogeography of the basins during the Late Neoproterozoic-Early Cambrian period. Stratigraphy, geochronological and paleomagnetic data: Marwar Supergroup – (Davis et al., 2014; McKenzie et al., 2011; Meert et al., 2013; Rathore et al., 1999 and present study); Huqf Supergroup – (Kilner et al., 2005; Le Guerroue, 2006; Rieu et al., 2007 and the references therein); Lesser Himalaya – (Jiang et al., 2003; Klootwijk, 1979; McKenzie et al., 2011; Tripathy and Singh, 2011 and the references therein). Yangtze block, South China – (Jiang et al., 2011, 2007, 2003; Macouin et al., 2004; Wang et al., 2012 and the references therein). Salt Range – (Gee, 1989; Krishnan, 1966; McElhinny, 1970).

of Pakistan (Gee, 1989; Krishnan, 1966). This marks the first phase in the evolution of the Marwar basin.

The second phase of the basin expansion started with the deepening of the basin and deposition of the Bilara carbonates at ~600 Ma (Fig. 13B), after a hiatus of ~100 Ma. The break in sedimentation also explains the lack of any physical evidence for the 635 Ma old, Marinoan Glaciation in the basin. The Hanseran Evaporite Group, a homotaxial equivalent of the Bilara Group (Das Gupta, 1996) is often correlated with contemporaneous evaporite deposits of the Ara Group in the Huqf Supergroup and Salt Range Formation (Saline Series) in the Salt Range (Fig. 14) owing to similarity in carbonate-evaporite cycles (Cozzi et al., 2012). In addition, Mazumdar and Strauss (2006) suggested that both Bilara and Hanseran Evaporate Groups could be coeval due to the similarity in their Sr and S isotopic ratios. The age of the Ara Group was constrained to be 544 ± 3 Ma (Brasier et al., 2000), and therefore, this age can be considered as the upper bound of the age of the Bilara Group. This protracted carbonate sedimentation period ends with the resumption of clastic sedimentation with the deposition of fluvial sandstones of the Nagaur Group (Fig. 13C). The youngest detrital zircon age of ~540 Ma (McKenzie et al., 2011) and trace fossil assemblages (Kumar and Pandey, 2010) reported from the Nagaur Formation suggest that its deposition occurred mostly in the Early Cambrian. These age constraints place the deposition of the Nagaur and Bilara Groups within the time frame of the Malagasy Orogeny when Indian shield collided with the already amalgamated Azania and Congo–Tanzania–Bangweulu Block in the final stages of formation of Gondwana (Collins and Pisarevsky, 2005; Meert, 2003). The relapse of sedimentation in the basin is associated with a change not only in the depositional facies but also in the provenance. According to earlier studies, the Nagaur sandstones show less matured character owing to shorter transportation and hence derivation from proximal sources (Pareek, 1984 and the references therein). Our geochemical data also capture this change in provenance (Fig. 12). From a BGC-2 dominant provenance, sediments became more confined to the sources in the Delhi Supergroup and/or Erinpura Granites suggesting a major tectonic event in the region during 700–600 Ma. Since NW India remained stable during the East African Orogeny (Collins and Pisarevsky, 2005), it is quite likely this event could be linked to the initial stages of the Malagasy Orogeny, where peak metamorphic conditions existed during 510–550 Ma (Ashwal et al., 2013; Rathore et al., 1999; Sen et al., 2013). The new age constraint provided by Sr isotopic stratigraphy makes the Gotan Limestone contemporaneous with a host of late Ediacaran carbonate successions (Fig. 14), such as the Khufai Formation of Oman, the lower gypsum dolomite stage of Salt Range, and lower part of the Krol Group and Doushantuo Formation of Lesser Himalayas and South China, respectively (Jiang et al., 2007; Le Guerroue, 2006; Tewari and Sial, 2007 and the references therein). Similarly, Early Cambrian Nagaur Group can be correlated with the top part of the Ara Group and the overlying Nimr Group, the Tal Group, Purple Sandstone and the Shuijingtuo/Niutitang Formation of Oman, Lesser Himalayas, Salt Range and the Yangtze block of South China, respectively (Fig. 14).

## 6. Conclusions

The age of formation of Chhoti Khatu rhyolitic tuff is determined to be 703 ± 40 (2σ) Ma, suggesting that the sedimentation in the basin started in the Cryogenian. Sr isotope stratigraphy suggests an approximate age of 570 Ma for the Gotan Formation of the Bilara Group suggesting a long depositional hiatus (~100 Ma) between the Jodhpur (~700 Ma) and Bilara (~570 Ma) Groups. The presence of this hiatus could be the reason for absence of any evidence for the Marinoan glaciation in the Marwar Basin. We propose a three phase evolution of the Marwar Basin: (1) formation of the basin subsequent to the disbanding of the Rodinia in the Cryogenian during which the deposition of Jodhpur Group took place, (2) deepening of the basin and carbonate deposition during and after the amalgamation of Gondwana in the Late Ediacaran, following a depositional haitus of ~100 Ma, and (3) deposition of fluvial sand in a shallow marginal basin during the Early Cambrian. Geochemistry of siliciclastic sediments in the Jodhpur Group suggests that they were primarily sourced from the Delhi Supergroup and the BGC-2, whereas the Bilara and Nagaur Groups formed from sediments from the Delhi Supergroup, with no sediment supply from the BGC-2. We find near absence of sediment supply from the Malani Igneous Suite except at the immediate contact regions with the bottommost Marwars.

## Acknowledgements

We thank Abhijit Basu and an anonymous reviewer for their constructive suggestions. We thank Mukund Sharma for introducing us to the Marwar Basin during a field workshop organized by him during January 2014. Anirban Chatterjee is thanked for his help during field trips and sampling.

## References

Ahmad, T., Dragusanu, C., Tanaka, T., 2008. Provenance of Proterozoic Basal Aravalli mafic volcanic rocks from Rajasthan, Northwestern India: Nd isotopes evidence for enriched mantle reservoirs. Precambr. Res. 162, 150–159.
Ashwal, L.D., Solanki, A.M., Pandit, M.K., Corfu, F., Hendriks, B.W.H., Burke, K., Torsvik, T.H., 2013. Geochronology and geochemistry of Neoproterozoic Mt. Abu granitoids, NW India: regional correlation and implications for Rodinia paleogeography. Precambr. Res. 236, 265–281.
Awasthi, A.K., Parkash, B., 1981. Depositional environments of unfossiliferous sediments of the Jodhpur Group, western India. Sed. Geol. 30, 15–42.
Bhowmik, S.K., Dasgupta, S., 2012. Tectonothermal evolution of the Banded Gneissic Complex in central Rajasthan, NW India: present status and correlation. J. Asian Earth Sci. 49, 339–348.
Biju-Sekhar, S., Yokoyama, K., Pandit, M.K., Okudaira, T., Yoshida, M., Santosh, M., 2003. Late Paleoproterozoic magmatism in Delhi Fold Belt, NW India and its implication: evidence from EPMA chemical ages of zircons. J. Asian Earth Sci. 22, 189–207.
Brasier, M., McCarron, G., Tucker, R., Leather, J., Allen, P., Shields, G., 2000. New U-Pb zircon dates for the Neoproterozoic Ghubrah glaciation and for the top of the Huqf Supergroup, Oman. Geology 28, 175–178.
Buick, I.S., Allen, C., Pandit, M., Rubatto, D., Hermann, J., 2006. The Proterozoic magmatic and metamorphic history of the Banded Gneiss Complex, central Rajasthan, India: LA-ICP-MS U-Pb zircon constraints. Precambr. Res. 151, 119–142.
Canfield, D.E., Poulton, S.W., Narbonne, G.M., 2007. Late-Neoproterozoic deep-ocean oxygenation and the rise of animal life. Science 315, 92–95.
Carter, L., 2005. Granitic and Rhyolitic Magmatism: Constraints on Continental Reconstruction from Geochemistry, Geochronology and Palaeomagnetism. M.Sc. Thesis (unpublished) Rand Afrikaans University, Johannesburg, pp. 1–54.
Chauhan, D.S., Mathur, K.M., Ram, N., 2001. Geological nature of the Pokaran boulder bed: paleoenvironmental, paleoclimatic and stratigraphic implications. J. Geol. Soc. India 58, 425–433.
Chauhan, D.S., Ram, B., Ram, N., 2004. Jodhpur sandstone: a gift of ancient beaches to western Rajasthan. J. Geol. Soc. India 64, 265–276.
Choudhary, A.K., 1984. Precambrian Geochronology of Rajasthan, Western India. Ph.D. Thesis Gujarat University, Ahmedabad, pp. 257.
Collins, A.S., Pisarevsky, S.A., 2005. Amalgamating eastern Gondwana: the evolution of the Circum-Indian Orogens. Earth Sci. Rev. 71, 229–270.
Cozzi, A., Rea, G., Craig, J., 2012. From global geology to hydrocarbon exploration: Ediacaran-Early Cambrian petroleum plays of India, Pakistan and Oman. Geol. Soc. Lond. Spec. Publ. 366, 131–162.
Crawford, A.R., Compston, W., 1970. The age of the Vindhyan system of Peninsular India. Quat. J. Geol. Soc. Lond. 125, 351–371.
Das Gupta, S.P., 1996. Marwar Supergroup evaporites, Rajasthan. In: Bhattacharya, A. (Ed.), Recent Advances in Vindhyan Geology. Memoirs – Geological Society of India 36, pp. 49–58.
Davis, J.K., Meert, J.G., Pandit, M.K., 2014. Paleomagnetic analysis of the Marwar Supergroup, Rajasthan, India and proposed interbasinal correlations. J. Asian Earth Sci. 91, 339–351.
Gee, E.R., 1989. Overview of the geology and structure of the Salt Range, with observations on related areas of northern Pakistan. Geol. Soc. Am. Spec. Pap. 232, 95–112.
Gopalan, K., Macdougall, J.D., Roy, A.B., Murali, A.V., 1990. Sm-Nd evidence for 3.3 Ga old rocks in Rajasthan, northwestern India. Precambr. Res. 48, 287–297.
Gregory, L.C., Meert, J.G., Bingen, B., Pandit, M.K., Torsvik, T.H., 2009. Paleomagnetism and geochronology of the Malani Igneous Suite, Northwest India: implications for the configuration of Rodinia and the assembly of Gondwana. Precambr. Res. 170, 13–26.
Halverson, G.P., Shields-Zhou, G., 2011. Chemostratigraphy and the Neoproterozoic glaciations. In: Arnaud, E., Halverson, G., Shields-Zhou, G. (Eds.), The Geological Record of Neoproterozoic Glaciations. Geological Society, London, pp. 51–66 Memoirs 36.
Hoffman, P.F., Kaufman, A.J., Halverson, G.P., Schrag, D.P., 1998. A Neoproterozoic snowball earth. Science 281, 1342–1346.
Jiang, G., Kaufman, A.J., Christie-Blick, N., Zhang, S., Wu, H., 2007. Carbon isotope variability across the Ediacaran Yangtze platform in South China: implications for a large surface-to-deep ocean $\delta^{13}C$ gradient. Earth Planet. Sci. Lett. 261, 303–320.
Jiang, G., Shi, X., Zhang, S., Wang, Y., Xiao, S., 2011. Stratigraphy and paleogeography of the Ediacaran Doushantuo Formation (ca. 635–551 Ma) in South China. Gondwana Res. 19, 831–849.
Jiang, G., Sohl, L.E., Christie-Blick, N., 2003. Neoproterozoic stratigraphic comparison of the Lesser Himalaya (India) and Yangtze block (south China): paleogeographic implications. Geology 31, 917–920.
Jochum, K.P., Nohl, U., Herwig, K., Lammel, E., Stoll, B., Hofmann, A.W., 2005. GeoReM: a new geochemical database for reference materials and isotopic standards. Geostand. Geoanal. Res. 29, 333–338.
Kaur, P., Chaudhri, N., Raczek, I., Kröner, A., Hofmann, A.W., 2007. Geochemistry, zircon ages and whole-rock Nd isotopic systematics for Palaeoproterozoic A-type granitoids in the northern part of the Delhi belt, Rajasthan, NW India: implications for late Palaeoproterozoic crustal evolution of the Aravalli craton. Geol. Mag. 144 (2), 361–378.
Kaur, P., Chaudhri, N., Raczek, I., Kröner, A., Hofmann, A.W., 2009. Record of 1.82 Ga Andean-type continental arc magmatism in NE Rajasthan, India: insights from zircon and Sm-Nd ages, combined with Nd-Sr isotope geochemistry. Gondwana Res. 16, 56–71.
Kaur, P., Chaudhri, N., Raczek, I., Kröner, A., Hofmann, A.W., Okrusch, M., 2011a. Zircon ages of late Palaeoproterozoic (ca. 1.72–1.70 Ga) extension-related granitoids in NE Rajasthan, India: regional and tectonic significance. Gondwana Res. 19, 1040–1053.
Kaur, P., Zeh, A., Chaudhri, N., Gerdes, A., Okrusch, M., 2011b. Archaean to Palaeoproterozoic crustal evolution of the Aravalli Mountain range, NW India, and its hinterland: the U-Pb and Hf isotope record of detrital zircon. Precambr. Res. 187, 155–164.
Kilner, B., Mac Niocaill, C., Brasier, M., 2005. Low-latitude glaciation in the Neoproterozoic of Oman. Geology 33, 413–416.
Klootwijk, C.T., 1979. A review of palaeomagnetic data from the Indo-Pakistani fragment of Gondwanaland. In: Farah, A., DeJong, K.A. (Eds.), Geodynamics of Pakistan. Geological Survey of Pakistan, Quetta, pp. 41–80.
Krishnan, M.S., 1966. Salt tectonics in the Punjab Salt Range, Pakistan. Geol. Soc. Am. Bull. 77, 115–122.
Kumar, S., Ahmad, S., 2014. Microbially induced sedimentary structures (MISS) from the Ediacaran Jodhpur Sandstone, Marwar Supergroup, western Rajasthan. J. Asian Earth Sci. 91, 352–361.
Kumar, S., Misra, P.K., Pandey, S.K., 2009. Ediacaran megaplant fossils with Vaucheriacean affinity from the Jodhpur Sandstone, Marwar Supergroup, western Rajasthan. Curr. Sci. 97, 701–705.
Kumar, S., Pandey, S.K., 2009. Note on the occurrence of Arumberia banksi and associated fossils from the Jodhpur sandstone, Marwar Supergroup, western Rajasthan. J. Palaeontol. Soc. India 54, 171–178.
Kumar, S., Pandey, S.K., 2010. Trace fossils from the Nagaur Sandstone, Marwar Supergroup, Dulmera area, Bikaner district, Rajasthan, India. J. Asian Earth Sci. 38, 77–85.
Kumar, V., 1999. Evolution and geological set-up of the Nagaur-Ganganagar Basin, northwestern Rajasthan. In: Paliwal, B.S. (Ed.), Geological Evolution of Northwestern India. Scientific Publishers, Jodhpur, India, pp. 34–60.
Le Guerroue, E., 2006. Sedimentology and Chemostratigraphy of the Ediacaran Shuram Formation, Nafun Group, Oman. Ph.D. Thesis Swiss Federal Institute of Technology, Zurich (ETHZ), pp. 1–209.
Li, Z.X., Bogdanova, S.V., Collins, A.S., Davidson, A., De Waele, B., Ernst, R.E., Fitzsimons, I.C.W., Fuck, R.A., Gladkochub, D.P., Jacobs, J., Karlstrom, K.E., Lu, S., Natapov, L.M., Pease, V., Pisarevsky, S.A., Thrane, K., Vernikovsky, V., 2008. Assembly, configuration, and break-up history of Rodinia: a synthesis. Precambr. Res. 160, 179–210.
Linnemann, U., Sharma, M., 2014. U-Pb LA-ICP-MS zircon ages from the Marwar Supergroup and its underlying basement. In: Sharma, M., Pandey, S.K., Kumar, S. (Eds.), International Field Workshop on the Marwar Supergroup, Rajasthan, India. The Society of Earth Scientists, India, pp. 76.
Ludwig, K.R., 2012. Isoplot v3.75, A Geochronological Toolkit for Excel. Berkeley Geochronology Center, Spec. Publ. No. 5. Berkeley Geochronological Centre, Berkeley, California, pp. 1–75.
Macouin, M., Besse, J., Ader, M., Gilder, S., Yang, Z., Sun, Z., Agrinier, P., 2004. Combined paleomagnetic and isotopic data from the Doushantuo carbonates, South

China: implications for the “snowball Earth” hypothesis. Earth Planet. Sci. Lett. 224, 387–398.
Malone, S.J., Meert, J.G., Banerjee, D.M., Pandit, M.K., Tamrat, E., Kamenov, G.D., Pradhan, V.R., Sohl, L.E., 2008. Paleomagnetism and detrital zircon geochronology of the upper Vindhyan sequence, son valley and Rajasthan, India: a ca. 1000 ma closure age for the purana basins? Precambr. Res. 164, 137–159.
Mazumdar, A., Bhattacharya, S.K., 2004. Stable isotopic study of late Neoproterozoic-early Cambrian (?) sediments from Naguar-Ganganagar basin, western India: possible signatures of global and regional C-isotopic events. Geochem. J. 38, 163–175.
Mazumdar, A., Strauss, H., 2006. Sulfur and strontium isotopic compositions of carbonate and evaporite rocks from the late Neoproterozoic–early Cambrian Bilara Group (Nagaur-Ganganagar Basin, India): constraints on intrabasinal correlation and global sulfur cycle. Precambr. Res. 149, 217–230.
McArthur, J.M., Howarth, R.J., Shields, G.A., 2012. Strontium isotope stratigraphy. In: Gradstein, F.M., Ogg, J.G., Schmitz, M.D., Ogg, G.M. (Eds.), The Geologic Time Scale. Elsevier, pp. 127–144.
McElhinny, M.W., 1970. Palaeomagnetism of the Cambrian purple sandstone from the Salt Range, West Pakistan. Earth Planet. Sci. Lett. 8, 149–156.
McFadden, K.A., Huang, J., Chu, X., Jiang, G., Kaufman, A.J., Zhou, C., Yuan, X., Xiao, S., 2008. Pulsed oxidation and biological evolution in the Ediacaran Doushantuo Formation. Proc. Natl. Acad. Sci. U.S.A. 105, 3197–3202.
McKenzie, N.R., Hughes, N.C., Myrow, P.M., Banerjee, D.M., Deb, M., Planavsky, N.J., 2013. New age constraints for the Proterozoic Aravalli-Delhi successions of India and their implications. Precambr. Res. 238, 120–128.
McKenzie, N.R., Hughes, N.C., Myrow, P.M., Xiao, S., Sharma, M., 2011. Correlation of Precambrian-Cambrian sedimentary successions across northern India and the utility of isotopic signatures of Himalayan lithotectonic zones. Earth Planet. Sci. Lett. 312, 471–483.
McLennan, S.M., Hemming, S., 1992. Samarium/neodymium elemental and isotopic systematics in sedimentary rocks. Geochim. Cosmochim. Acta 56, 887–898.
Meert, J.G., 2003. A synopsis of events related to the assembly of the eastern Gondwana. Tectonophysics 362, 1–40.
Meert, J.G., Pandit, M.K., Kamenov, G.D., 2013. Further geochronological and paleomagnetic constraints on Malani (and pre-Malani) magmatism in NW India. Tectonophysics 608, 1254–1267.
Och, L.M., Shields-Zhou, G.A., 2012. The Neoproterozoic oxygenation event: environmental perturbations and biogeochemical cycling. Earth Sci. Rev. 110, 26–57.
Paliwal, B.S., 1998. Felsic volvanics interlayered with sediments of the Marwar Supergroup of Chhoti Khatu, District Nagaur, Rajasthan. J. Geol. Soc. India 52, 81–86.
Pandey, D.K., Bahadur, T., 2009. A review of the stratigraphy of Marwar Supergroup of west-central Rajasthan. J. Geol. Soc. India 73, 747–758.
Pandit, M.K., Carter, L.M., Ashwal, L.D., Tucker, R.D., Torsvik, T.H., Jamtveit, B., Bhushan, S.K., 2003. Age, petrogenesis and significance of 1 Ga granitoids and related rocks from the Sendra area, Aravalli Craton, NW India. J. Asian Earth Sci. 22, 363–381.
Pandit, M.K., Sial, A.N., Jamrani, S.S., Ferreira, V.P., 2001. Carbon isotopic profile across the Bilara group rocks of trans-Aravalli Marwar Supergroup in Western India: implications for Neoproterozoic—Cambrian Transition. Gondwana Res. 4, 387–394.
Pareek, H.S., 1981. Basin configuration and sedimentary stratigraphy of western Rajasthan. J. Geol. Soc. India 22, 517–527.
Pareek, H.S., 1984. Pre-Quaternary geology and mineral resources of northwestern Rajasthan. Geol. Surv. India – Memoirs 115, 1–99.
Purohit, R., Papineau, D., Kröner, A., Sharma, K.K., Roy, A.B., 2012. Carbon isotope geochemistry and geochronological constraints of the Neoproterozoic Sirohi Group from northwest India. Precambr. Res. 220–221, 80–90.
Raghav, K.S., De, C., Jain, R.L., 2005. The first record of Vendian Medusoids and trace fossil-bearing algal matgrounds from the basal part of the Marwar Supergroup of Rajasthan, India. Indian Miner. 59, 23–30.
Rathore, S.S., Venkatesan, T.R., Srivastava, R., 1999. Rb-Sr isotope dating of Neoproterozoic (Malani Group) magmatism from Southwest Rajasthan, India: evidence of younger Pan-African thermal event by $^{40}$Ar-$^{39}$Ar studies. Gondwana Res. 2, 271–281.
Rathore, S.S., Venkatesan, T.R., Srivastava, R.K., 1996. Rb-Sr and Ar-Ar systematics of Malani volcanic rocks of southwest Rajasthan: evidence for a younger post-crystallization thermal event. Proc. Indian Acad. Sci. (Earth Planet. Sci.) 105, 131–141.
Ray, J.S., Veizer, J., Davis, W.J., 2003. C, O, Sr and Pb isotope systematics of carbonate sequences of the Vindhyan Supergroup, India: age, diagenesis, correlations and implications for global events. Precambr. Res. 121, 103–140.
Rieu, R., Allen, P.A., Cozzi, A., Kosler, J., Bussy, F., 2007. A composite stratigraphy for the Neoproterozoic Huqf Supergroup of Oman: integrating new litho-, chemo- and chronostratigraphic data of the Mirbat area, southern Oman. J. Geol. Soc. Lond. 164, 997–1009.
Roy, A.B., Jakhar, S.R., 2002. Geology of Rajasthan (Northwest India): Precambrian to Recent. Scientific Publishers, Jodhpur, India, pp. 1–421.
Roy, A.B., Kröner, A., 1996. Single zircon evaporation ages constraining the growth of the Archaean Aravalli craton, northwestern Indian shield. Geol. Mag. 133, 333–342.
Roy, A.B., Kröner, A., Bhattachaya, P.K., Rathore, S., 2005. Metamorphic evolution and zircon geochronology of early Proterozoic granulites in the Aravalli Mountains of northwestern India. Geol. Mag. 142, 287–302.
Sarkar, S., Bose, P., Samanta, P., Sengupta, P., Eriksson, P., 2008. Microbial mat mediated structures in the Ediacaran Sonia Sandstone, Rajasthan, India, and their implications for proterozoic sedimentation. Precambr. Res. 162, 248–263.
Sen, A., Pande, K., Sheth, H.C., Sharma, K.K., Sarkar, S., Dayal, A.M., Mistry, H., 2013. An Ediacaran-Cambrian thermal imprint in Rajasthan, western India: evidence from $^{40}$Ar-$^{39}$Ar geochronology of the Sindreth volcanics. J. Earth Syst. Sci. 122, 1477–1493.
Sun, S.-s., McDonough, W.F., 1989. Chemical and isotopic systematics of oceanic basalts: implications for mantle composition and processes. In: Saunders, A.D., Norry, M.J. (Eds.), Magmatism in the Ocean Basins. Geological Society, London, Special Publications 42, pp. 313–345.
Tewari, V.C., Sial, A.N., 2007. Neoproterozoic-Early Cambrian isotopic variation and chemostratigraphy of the Lesser Himalaya, India, Eastern Gondwana. Chem. Geol. 237, 82–106.
Tobisch, O.T., Collerson, K.D., Bhattacharyya, T., Mukhopadhyay, D., 1994. Structural relationships and Sr-Nd isotope systematics of polymetamorphic granitic gneisses and granitic rocks from central Rajasthan, India: implications for the evolution of the Aravalli craton. Precambr. Res. 65, 319–339.
Torsvik, T.H., Carter, L.M., Ashwal, L.D., Bhushan, S.K., Pandit, M.K., Jamtveit, B., 2001. Rodinia refined or obscured: palaeomagnetism of the Malani igneous suite (NW India). Precambr. Res. 108, 319–333.
Tripathy, G.R., Singh, S.K., 2011. Re-Os isotopes and redox-sensitive elements of the Himalayan black shales: implications to marine anoxia near the Pc-C boundary. Mineral. Mag. 75 (3), 2031.
Turner, C.C., Meert, J.G., Pandit, M.K., Kamenov, G.D., 2014. A detrital zircon U-Pb and Hf isotopic transect across the Son Valley sector of the Vindhyan Basin, India: implications for basin evolution and paleogeography. Gondwana Res. 26, 348–364.
Van Lente, B., Ashwal, L.D., Pandit, M.K., Bowring, S.A., Torsvik, T.H., 2009. Neoproterozoic hydrothermally altered basaltic rocks from Rajasthan, northwest India: implications for late Precambrian tectonic evolution of the Aravalli Craton. Precambr. Res. 170, 202–222.
Wang, X., Shi, X., Jiang, G., Zhang, W., 2012. New U-Pb age from the basal Niutitang Formation in South China: implications for diachronous development and condensation of stratigraphic units across the Yangtze platform at the Ediacaran-Cambrian transition. J. Asian Earth Sci. 48, 1–8.
Wiedenbeck, M., Goswami, J.N., 1994. High precision $^{207}$Pb/$^{206}$Pb zircon geochronology using a small ion microprobe. Geochim. Cosmochim. Acta 58, 2135–2141.
Wiedenbeck, M., Goswami, J.N., Roy, A.B., 1996. Stabilization of the Aravalli Craton of northwestern India at 2.5 Ga: an ion microprobe zircon study. Chem. Geol. 129, 325–340.
Xu, H., Meert, J.G., 2014. New ICP-MS U-Pb zircon ages from Khatu Rhyolites in the Jodhpur Group, India: constraints on the lower age limit for the Marwar Supergroup. In: AGU Fall Meeting Abstracts. AGU, pp. 3560.
Yang, Y.H., Chu, Z.Y., Wu, F.Y., Xie, L.W., Yang, J.H., 2011. Precise and accurate determination of Sm, Nd concentrations and Nd isotopic compositions in geological samples by MC-ICP-MS. J. Anal. At. Spectrom. 26, 1237–1244.